Fig. 2-4-16坑井 AMJ-2 注水試験記録

Flow rate and pressure data, Well AMJ-2 injectivity test

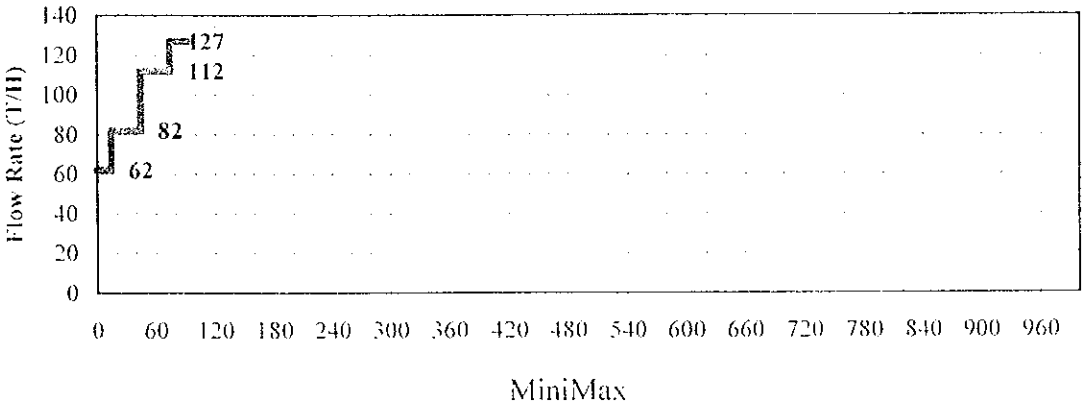

MiniMax

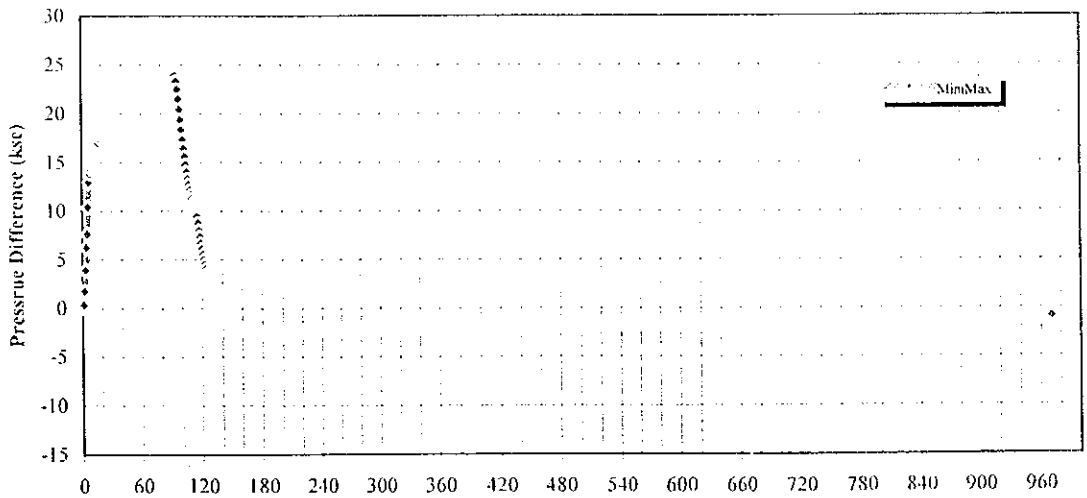

Fig. 2-4-16坑井 AMJ-2 注水試験記録

Flow rate and pressure data, Well AMJ-2 injectivity test

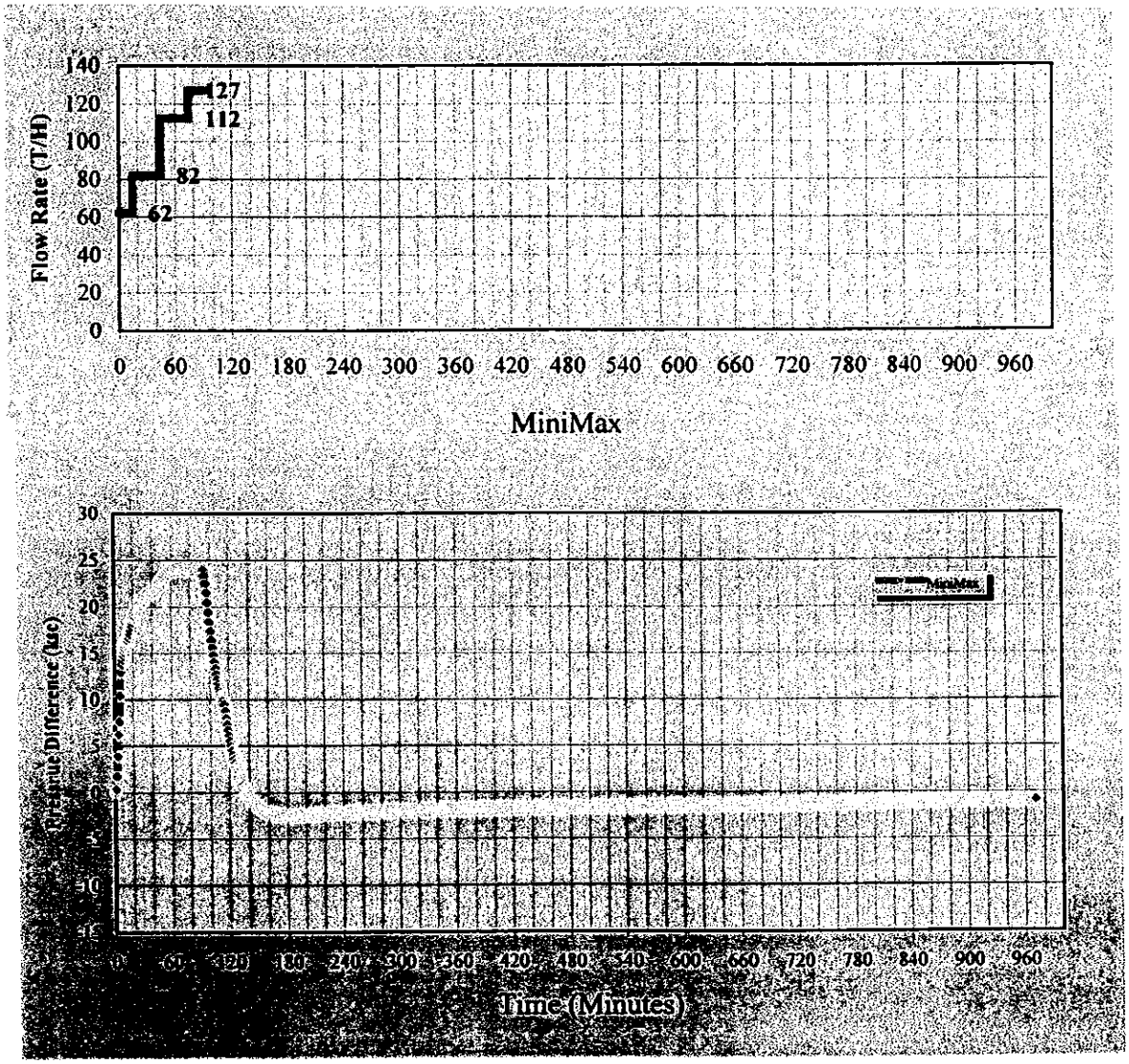

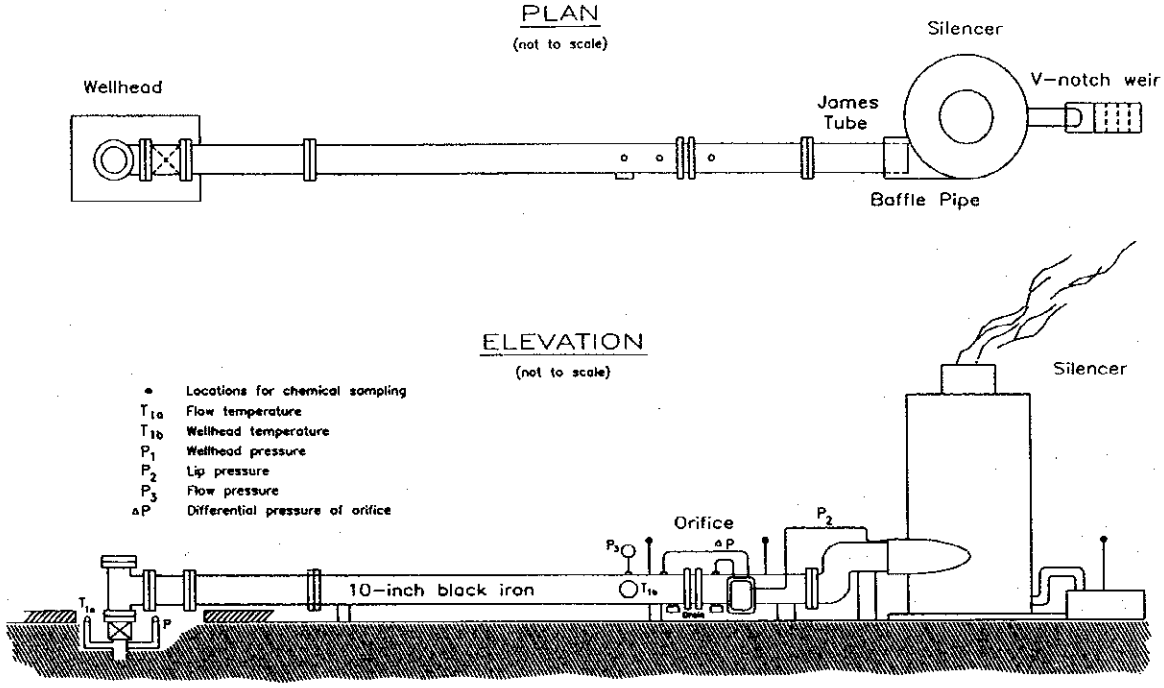

Fig. 2-4-17 Well setup for the "James" Lip Pressure Method

リッププレッシャー法試験設備

坑井AMJ-1の第1回噴出試験結果

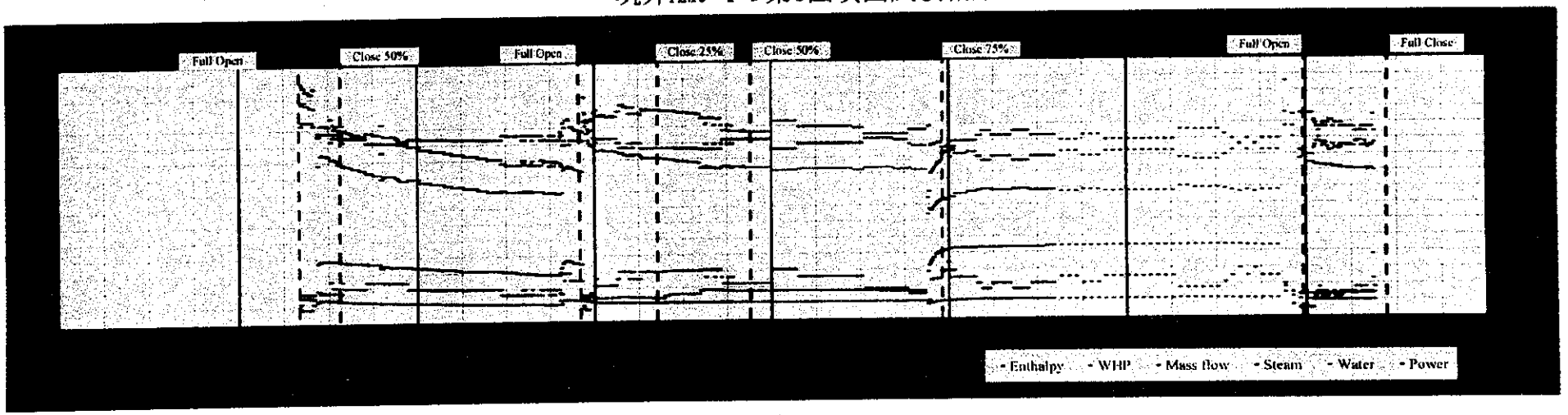

坑井AMJ-1の第1回噴出試験結果

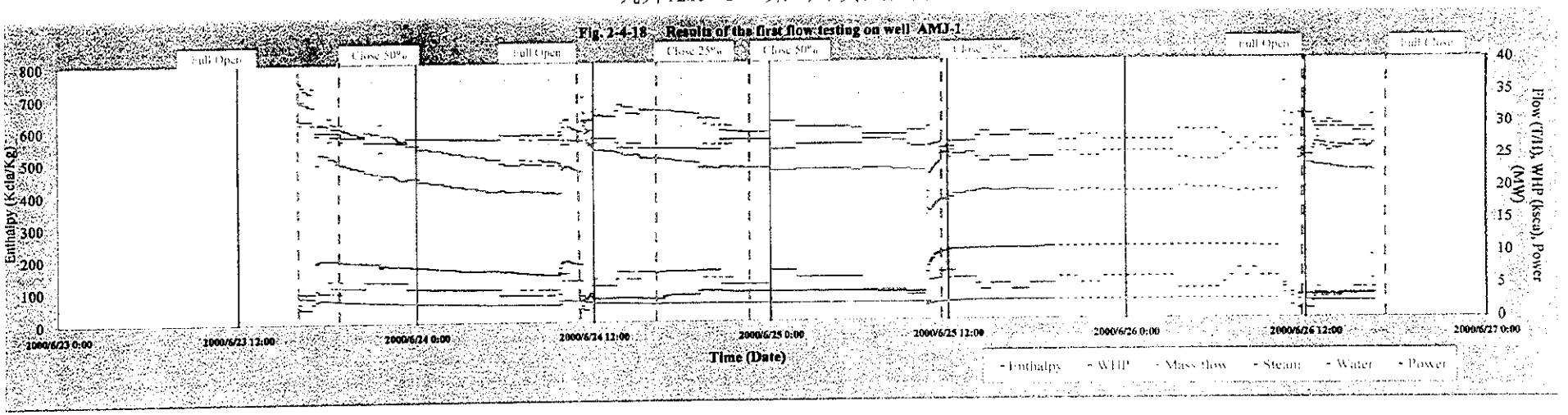

Fig. 2-4-18 Results of the first flow testing on well AMJ-1

坑井AMJ-1の第1回噴出試験の坑井特性

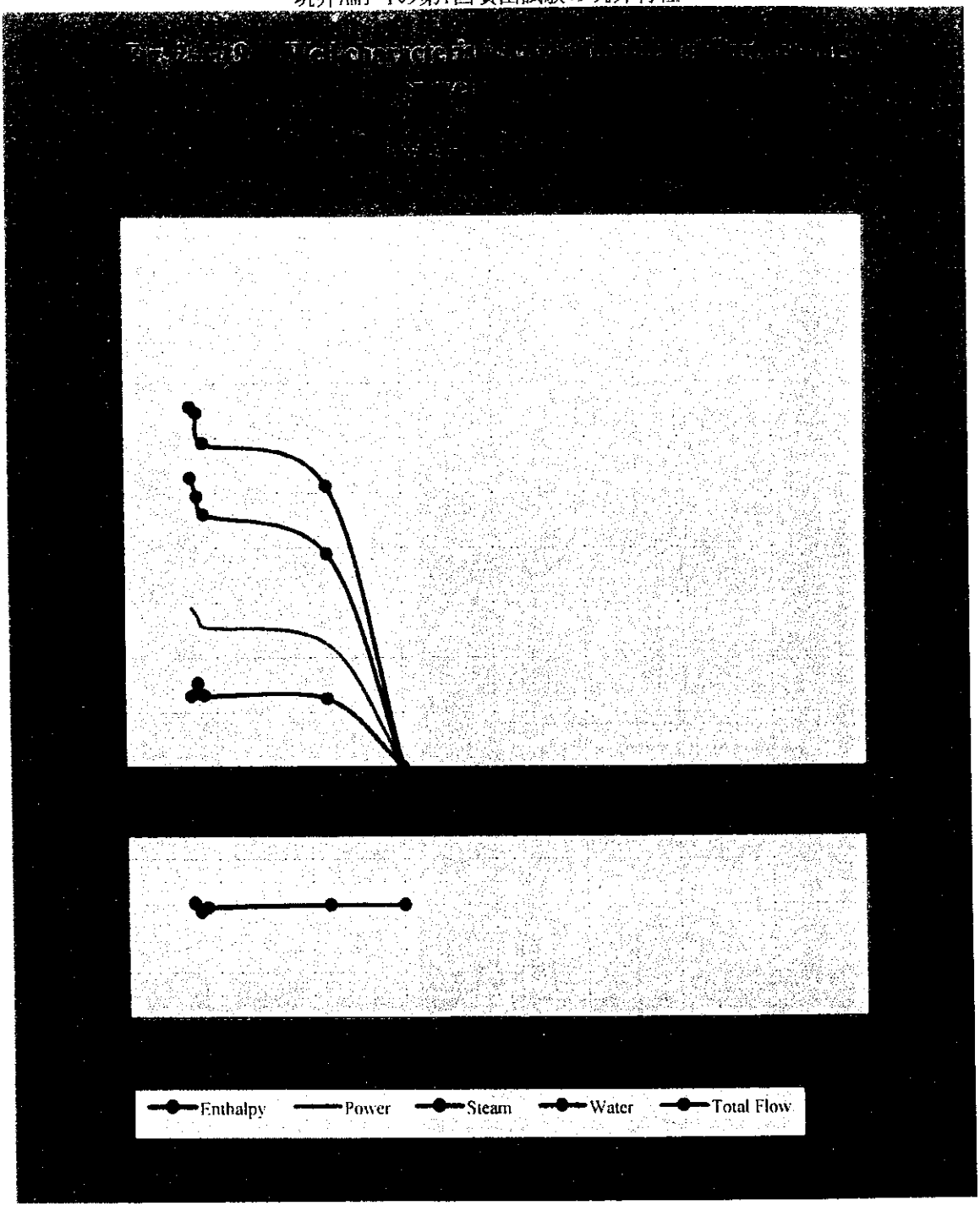

坑井AMJ-1の第1回噴出試験の坑井特性

Fig. 2-4-19 Well characteristic curve for the 1st flow testing on well AMJ-1

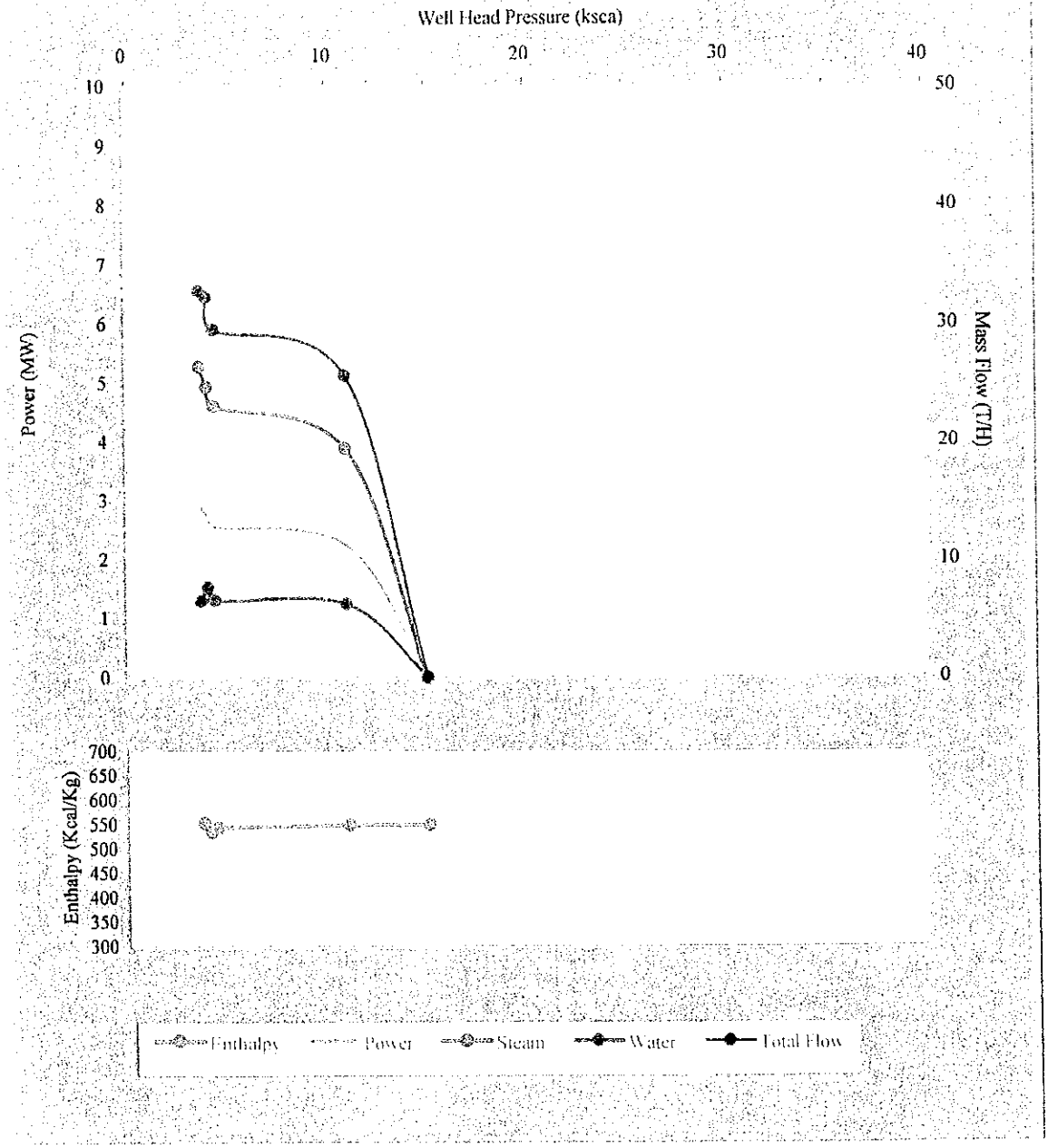

坑井AMJ-1の第2回噴出試験結果

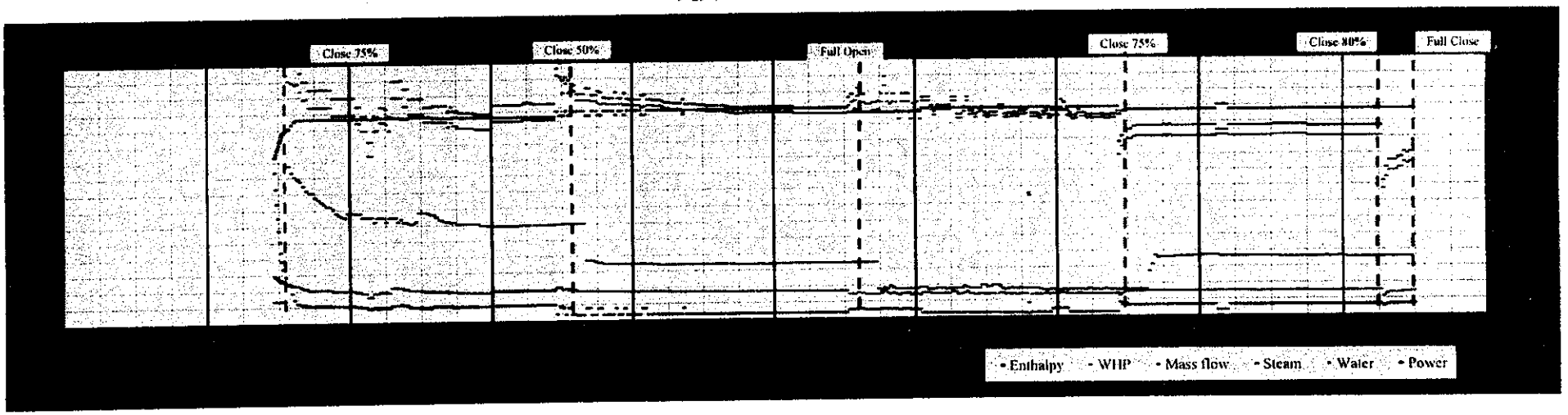

坑井AMJ-1の第2回噴出試験結果

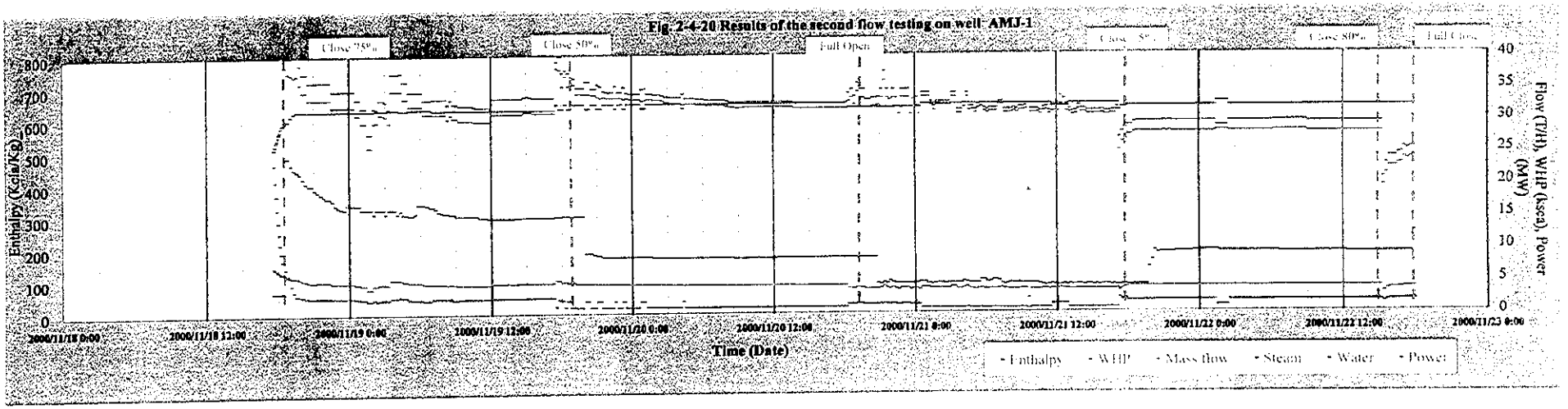

Fig. 2-4-20 Results of the second flow testing on well AMJ-1

坑井AMJ-1の第2回噴出試験の坑井特性

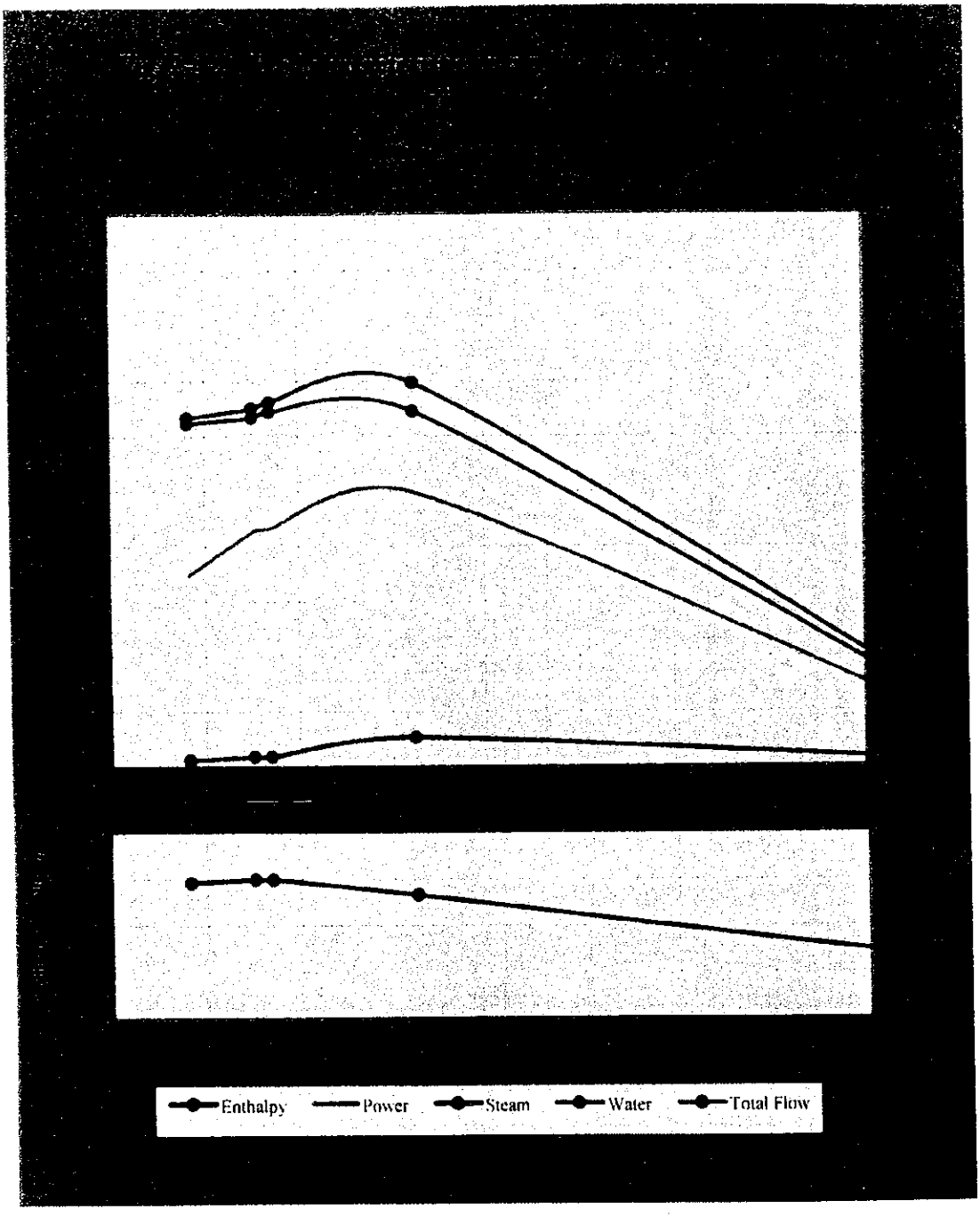

Fig. 2-4-21 Well characteristic curve for the 2nd. flow testing on well AMJ-1

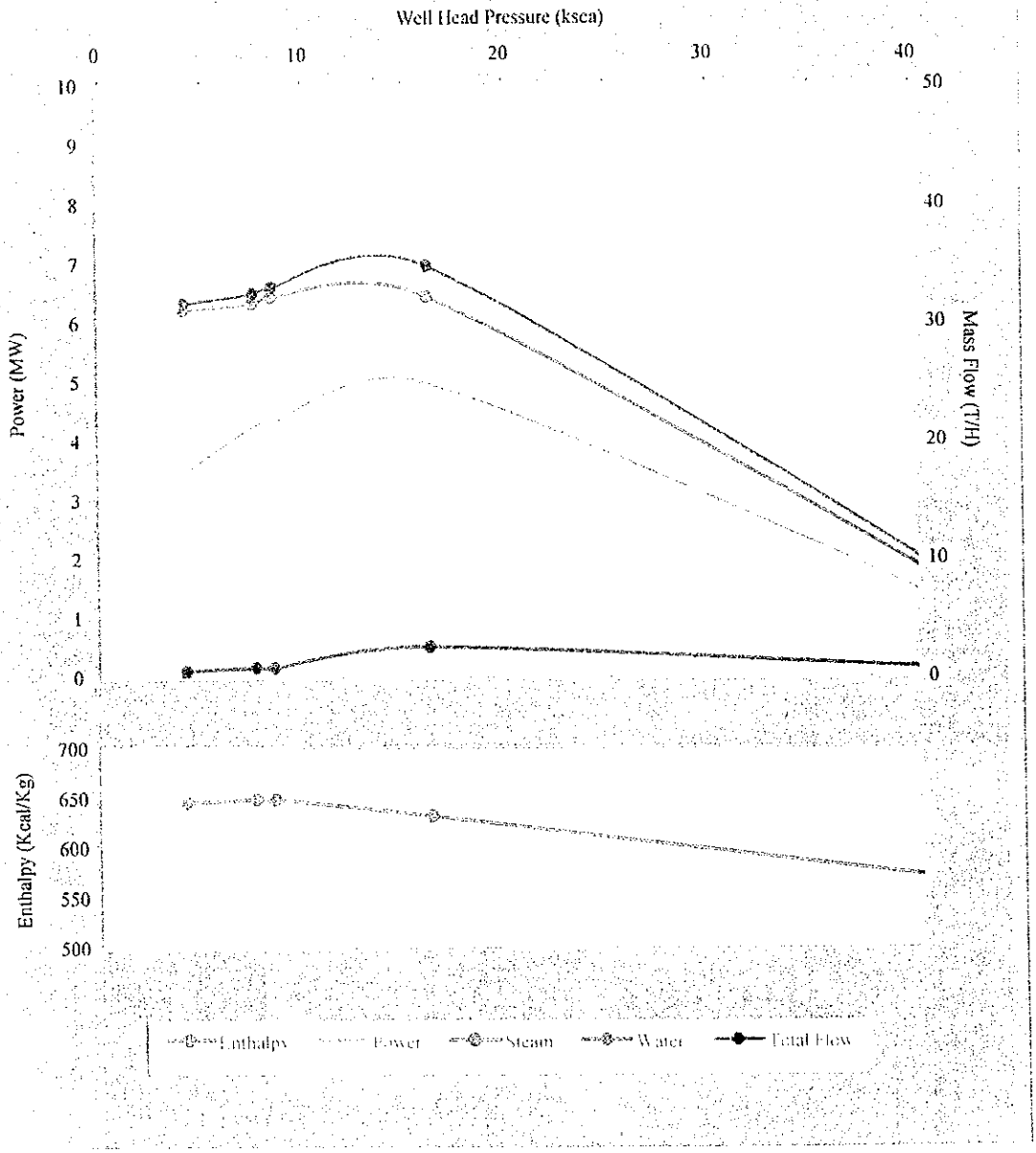

坑井AMJ-2の第1回噴出試験結果

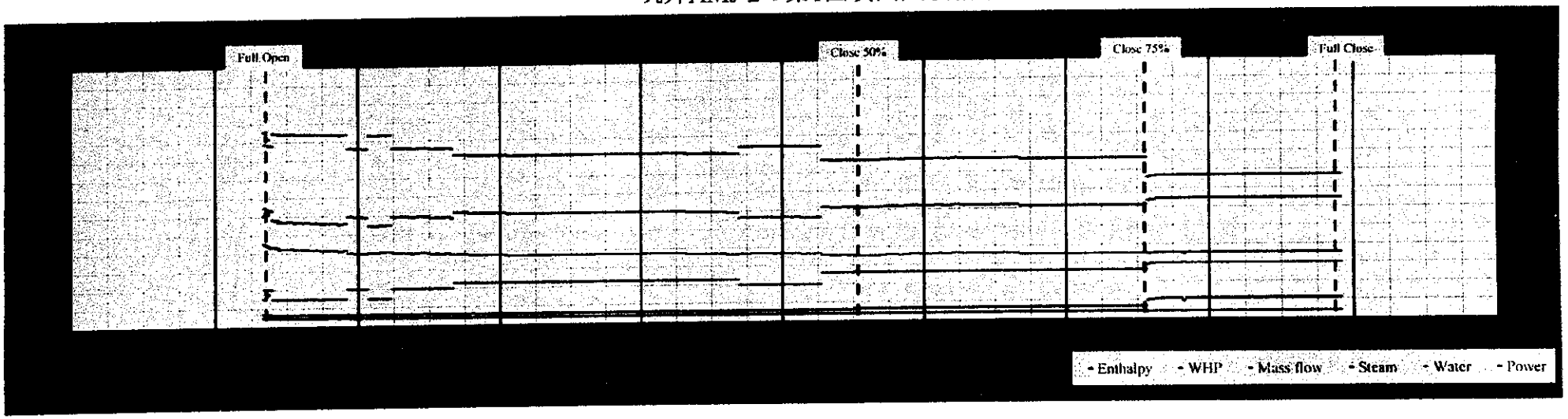

坑井AMJ-2の第1回噴出試験結果

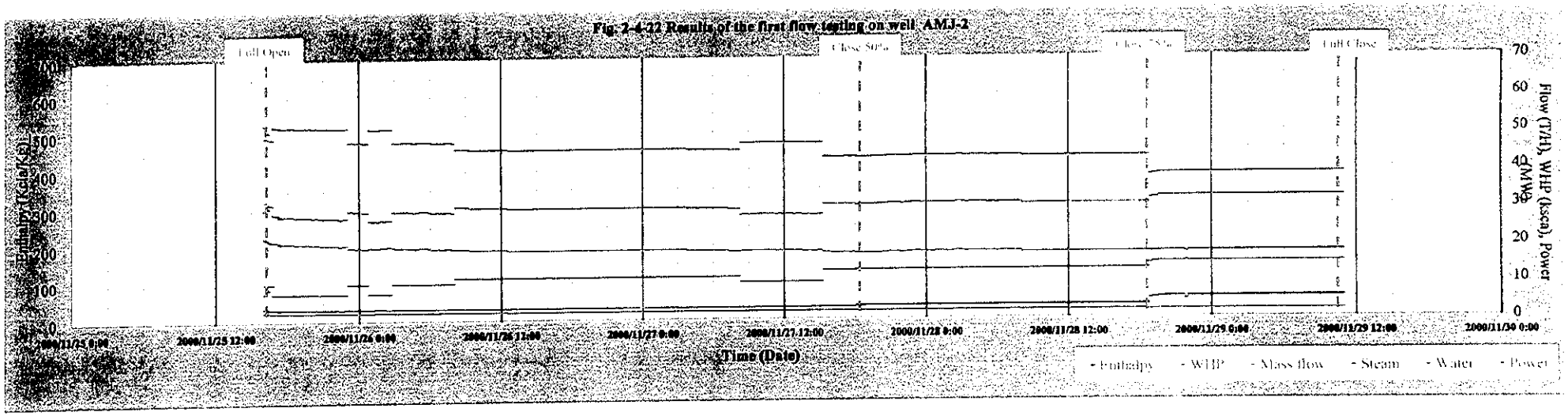

坑井AMJ-2の第１回噴出試験の坑井特性

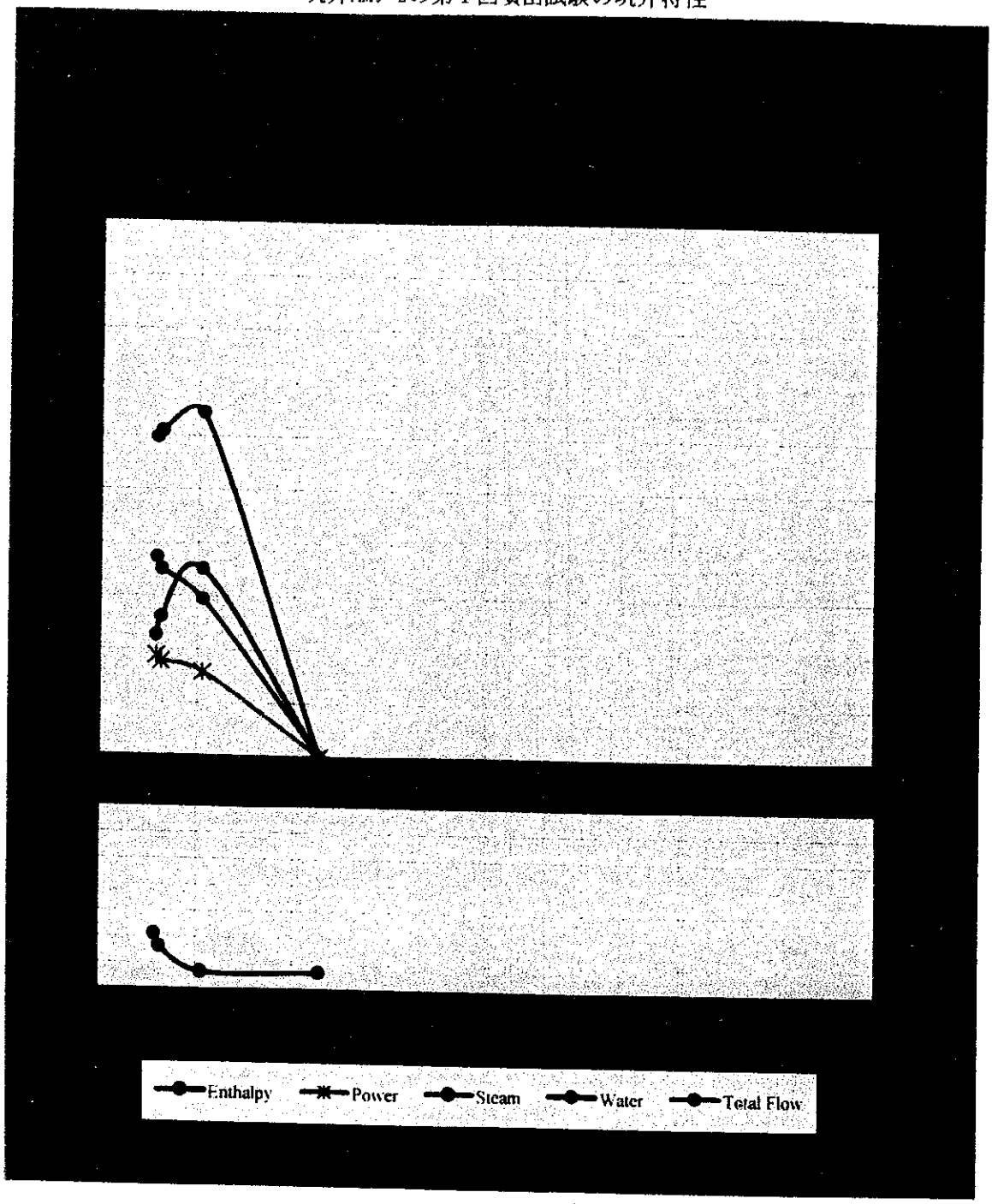

Fig. 2-4-23 Well characteristic curve for the 1st flow testing on well AMJ-2

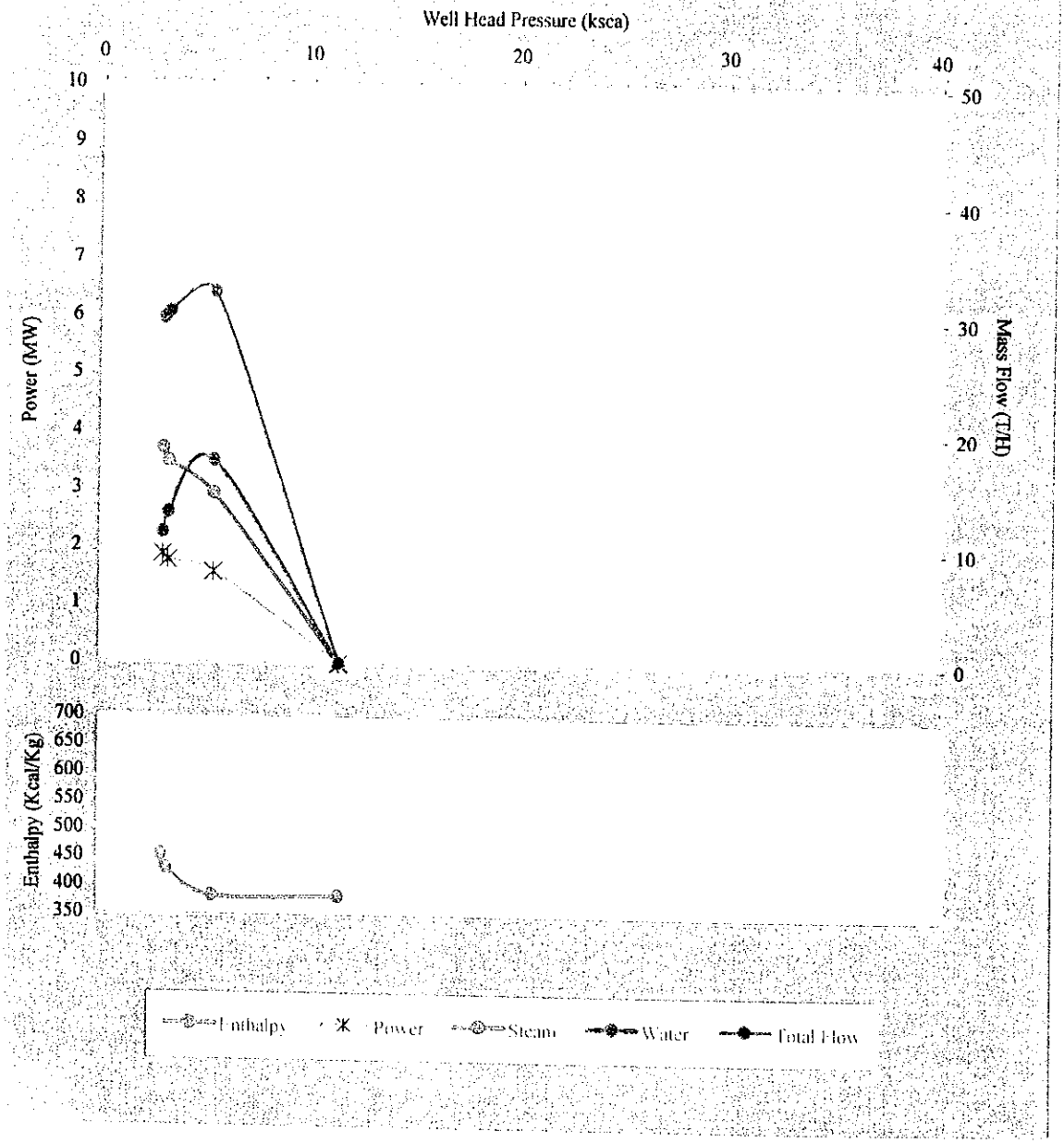

坑井AMJ-2の第2回噴出試験結果

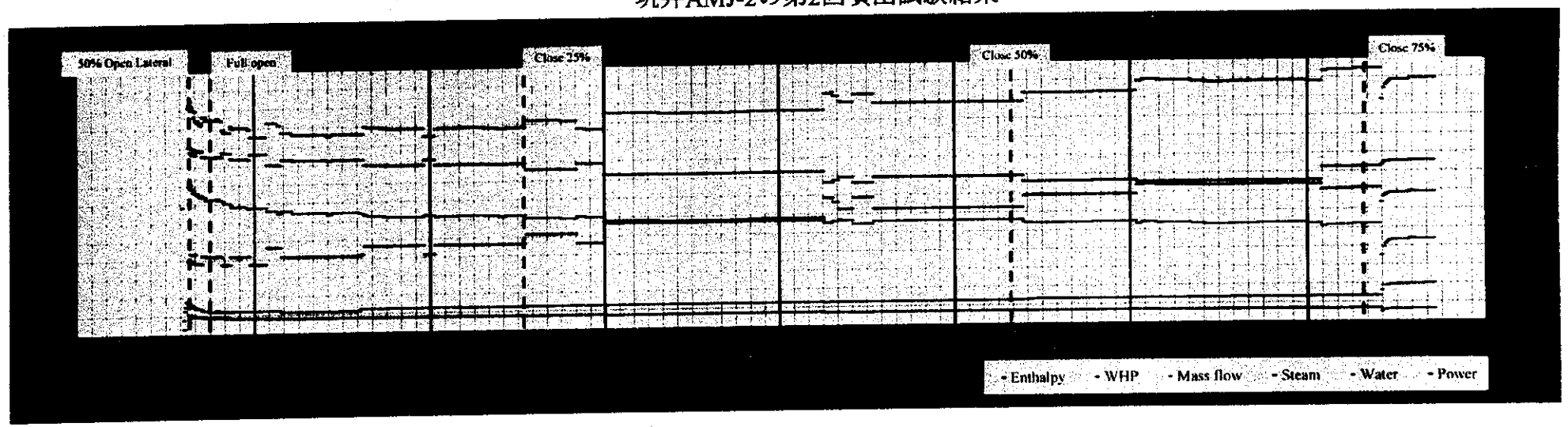

坑井AMJ-2の第2回噴出試験結果

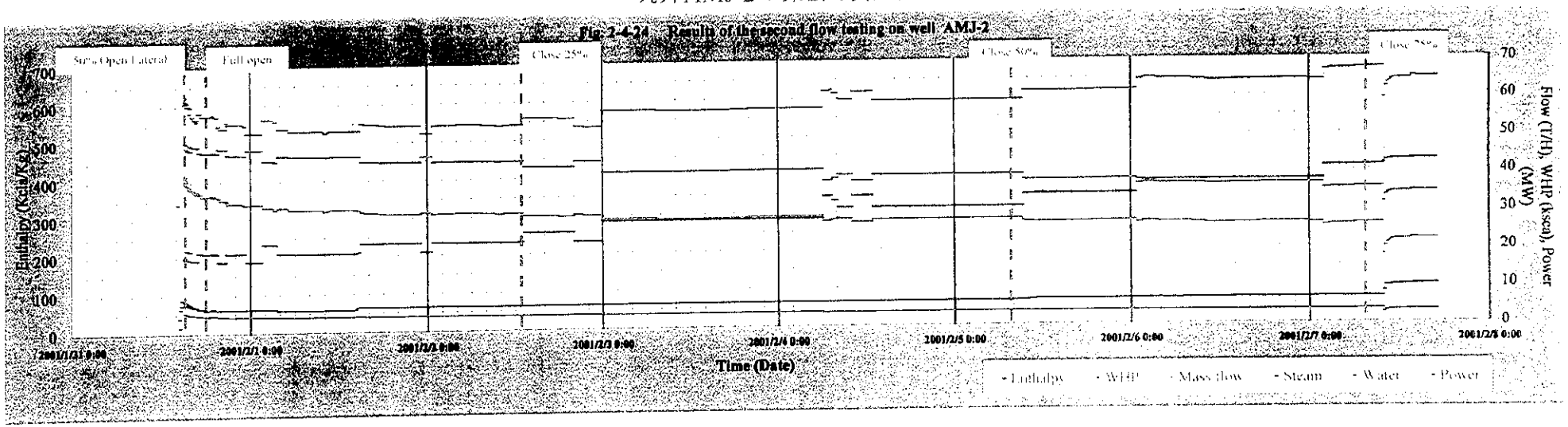

坑井AMJ-2の第２回噴出試験の坑井特性

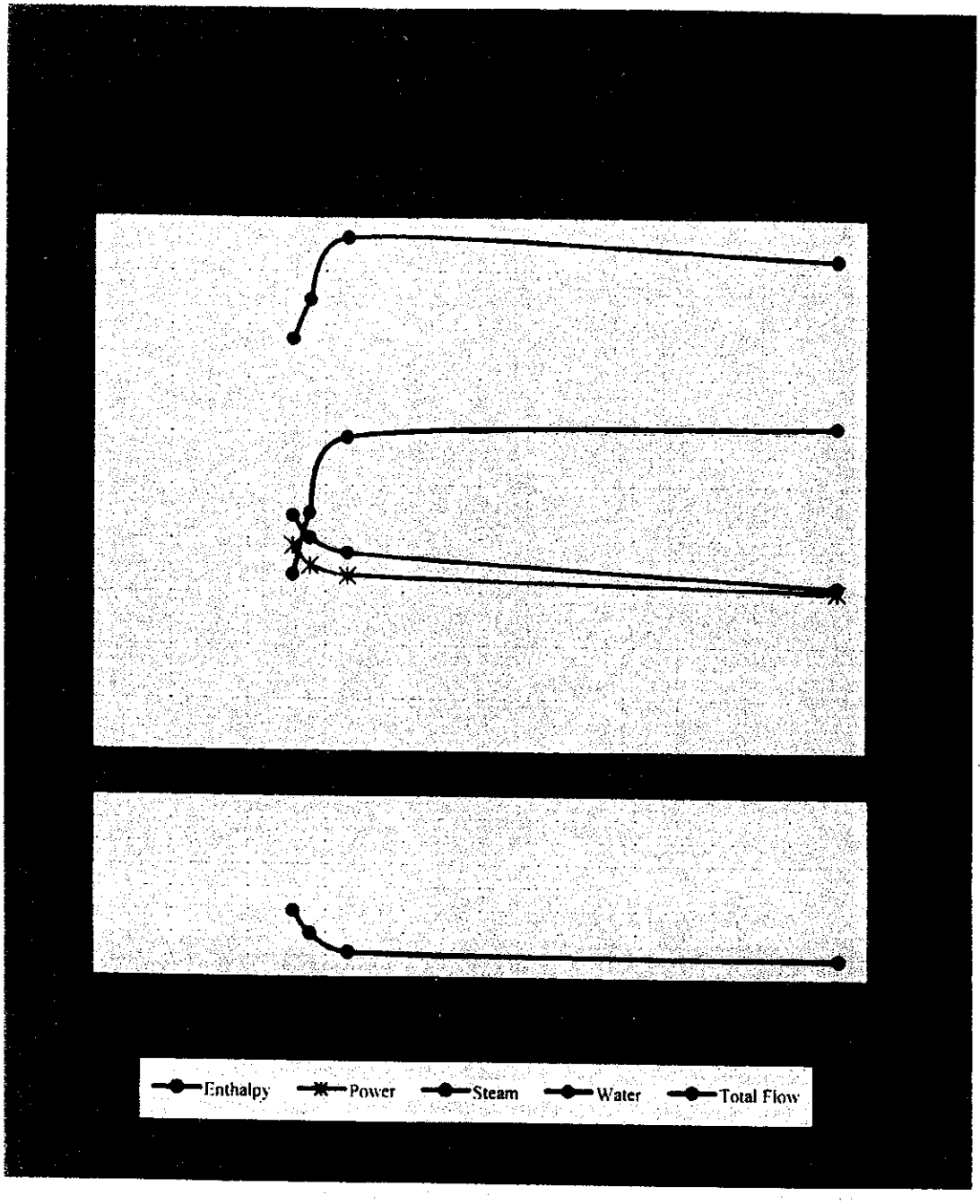

坑井AMJ-2の第２回噴出試験の坑井特性

Fig. 2-4-25 Well characteristic curve for the 2nd. flow testing on well AMJ-2

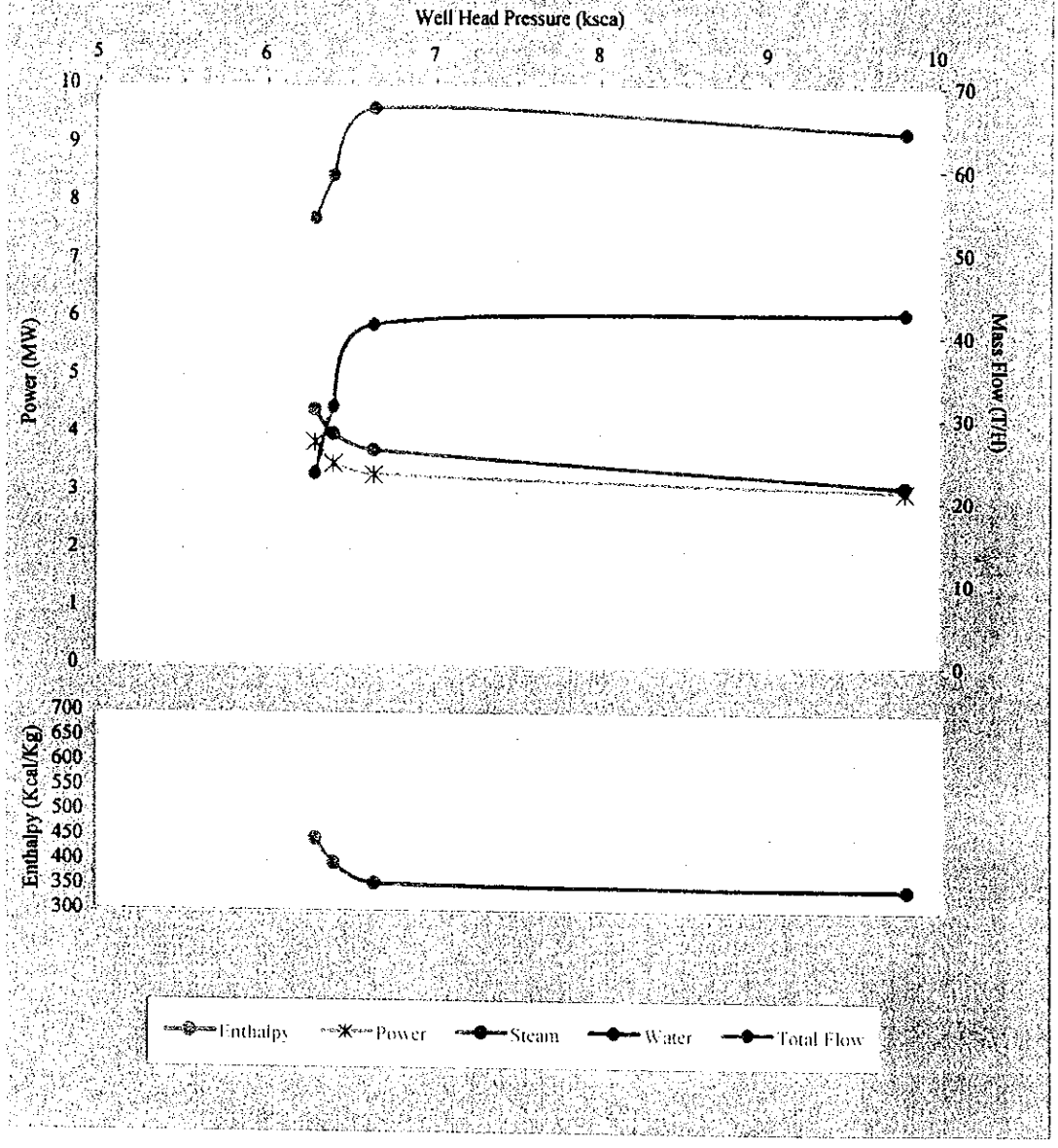

Table 2-4-1 Morphological Data on Zircon
ジルコン結晶系解析結果

Sample No.	Width (mm)	Height (mm)	Prism Index	Pyramid Index	Elongation Index	Flatness Indes	Zircon Index	Remark
1602	0.045±0.014	0.120±0.055	0.68±0.16	0.43±0.10	0.39±0.12	0.87±0.14	7449(45)	from outcrop
1611	0.026±0.007	0.055±0.016	0.58±0.15	0.39±0.08	0.33±0.14	0.90±0.06	6439(26)	from outcrop
1703	0.043±0.019	0.102±0.037	0.71±0.13	0.41±0.12	0.40±0.10	0.92±0.05	7449(43)	from outcrop
1901	0.049±0.010	0.093±0.024	0.69±0.10	0.35±0.06	0.32±0.07	0.93±0.09	7439(49)	from outcrop
2003	0.027±0.006	0.051±0.018	0.62±0.11	0.36±0.09	0.28±0.14	0.86±0.10	6439(27)	from outcrop
2101	0.046±0.018	0.056±0.026	0.61±0.06	0.33±0.17	0.21±0.05	0.92±0.06	6329(46)	from outcrop
2215	0.046±0.016	0.112±0.057	0.76±0.09	0.47±0.07	0.31±0.13	0.94±0.03	8539(46)	from outcrop
2506	0.057±0.011	0.100±0.023	0.73±0.10	0.42±0.05	0.22±0.06	0.94±0.04	7429(57)	from outcrop
2803	0.050±0.013	0.112±0.038	0.72±0.09	0.50±0.08	0.27±0.08	0.90±0.07	7539(50)	from outcrop
2806	0.048±0.013	0.098±0.039	0.66±0.08	0.44±0.13	0.27±0.19	0.94±0.04	7439(48)	from outcrop
1902	-	-	-	-	-	-	Zr-free	from outcrop
2402	-	-	-	-	-	-	Zr-free	from outcrop
2812	-	-	-	-	-	-	Zr-free	from outcrop
Cerro Limon	0.066±0.019	0.158±0.043	0.75±0.13	0.47±0.07	0.36±0.11	0.81±0.11	8548(66)	from outcrop, *1)
Amatitlan	0.090±0.016	0.174±0.037	0.54±0.23	0.33±0.05	0.35±0.07	0.89±0.08	5349(90)	from outcrop, *1)
AMF-1-150m	0.081±0.021	0.168±0.028	0.62±0.10	0.44±0.05	0.30±0.11	0.88±0.09	6439(81)	*1)
AMF-2-140m	0.078±0.022	0.159±0.020	0.60±0.12	0.43±0.04	0.34±0.14	0.92±0.04	6439(78)	*1)
AMF-2-550m	0.060±0.011	0.116±0.018	0.79±0.14	0.40±0.08	0.30±0.05	0.93±0.06	8439(60)	*1)
AMF-3-50m	0.076±0.010	0.162±0.017	0.83±0.05	0.42±0.07	0.34±0.08	0.91±0.06	8439(76)	*1)
AMF-3-100m	-	-	-	-	-	-	Zr-free	*1)
AMF-3-1000m	-	-	-	-	-	-	Zr-free	*1)
AMF-4-160m	-	-	-	-	-	-	Zr-free	*1)
AMF-4-1000m	-	-	-	-	-	-	Zr-free	*1)
AMF-4-1300m	0.069±0.015	0.168±0.043	0.46±0.21	0.39±0.09	0.39±0.10	0.88±0.09	5449(69)	*1)
AMJ-1-310m	0.083±0.019	0.186±0.059	0.73±0.09	0.47±0.05	0.40±0.09	0.90±0.07	7549(30)	
AMJ-1-410m	0.075±0.018	0.148±0.041	0.73±0.05	0.44±0.06	0.37±0.08	0.90±0.05	7449(13)	
AMJ-1-1130m	0.057±0.011	0.159±0.041	0.63±0.07	0.47±0.08	0.48±0.13	0.89±0.03	6559(10)	
AMJ-1-1630m	0.099±0.017	0.234±0.089	0.60±0.21	0.45±0.09	0.40±0.09	0.86±0.10	6549(30)	
AMJ-1-1700m	0.105±0.029	0.224±0.055	0.37±0.17	0.31±0.08	0.44±0.08	0.85±0.10	4349(40)	
AMJ-2-190m	0.049±0.006	0.102±0.024	0.75±0.09	0.46±0.07	0.40±0.06	0.91±0.07	8549(17)	
AMJ-2-300m	0.081±0.016	0.176±0.051	0.74±0.09	0.48±0.04	0.39±0.08	0.90±0.08	7549(50)	
AMJ-2-440m	0.082±0.026	0.162±0.052	0.73±0.08	0.43±0.06	0.40±0.09	0.89±0.07	7449(14)	
AMJ-2-1250m	0.099±0.013	0.228±0.049	0.65±0.18	0.44±0.08	0.42±0.09	0.93±0.05	7449(13)	
AMJ-2-1650m	0.080±0.017	0.191±0.042	0.73±0.09	0.45±0.05	0.45±0.08	0.87±0.06	7559(80)	

*1) : Reported in West JEC and Telectro (1995)

Table 2-4-2 Volocanic and Alteration Age around the Amatitlan Geothermal Field
Amatitlan地熱地帯周辺の岩石および変質年代

	Outcrop No.	Depth(m) AMJ-1	AMJ-2	AMF-1	AMF-2	AMF-3	Dating(ka) F/T	K-Ar	T/L Dating(ka) (Volcanic)	(Alteration)
Cerro Limon Dacite									6.1±0.5	
Pacaya Volocanic Rocks										
Op Andesite	2402								8±2	
Op Andesite	2806								9±2	
Op Andesite	2812								4±1	
Basalt			130m						11±2	
Basalt			190m				270±110			
Px-Andesite		150m							11±2	
Post-Calderic Rocks										
Rd Acidic Andesite	1602						80±60			
(dacite)		310m					180±80			
(dacite)			300m				600±140			3.2±0.4
Sf Pumice	2003						150±80		92±10	
	2208									16±4
Bl Scoria										
Lp Pyroclastics										
		410m					340±140			5±1
Ap Pyroclastics	1611						110±60		55±5	
Tuff Breccia				150m				11000±9400		
Hv Andesite										
Av Px-Andesite	1703						1060±220			
	2803						1160±110			
			440m				900±260			4.7±0.6
					140m			14100±9000		
	2206									35±5
	2215									46±6
	2217									5±1
	2805									3±1
Syn-Calderic Rocks										
		780m					1140±310			
		1130m					>3600			
Pre-Calderic Rocks										
Ho-Andesite			1250m				>2690			
Px-Andesite			1650m				>16100			
Px-Andesite						1300m	14100±800			
Dacite		1630m					>11700			
Basement	Granite						15200±800			

Table 2-4-3 Results of X-ray Diffraction Analysis of Well AMJ-1

坑井AMJ－1におけるX線回折解析結果

Depth	Alteration Minerals																												Relics				
	I				II	III				IV					V							Others											
	Opal	Tridymite	Cristobaliste	Quartz	Alunite	Halloysite	Kaolinite	Dickite	Pyrophyllite	Smectiete	Chl./Smect.	Mica/Smect.	Chlorite	Sericite	Stiblite	Heulandite	Mordenite	Laumontite	Mairekite	Na-feldspar	K-feldspar	Gypsum	Anhydrite	Calcite	Pyrite	Hematite	Gibbsite	Epidote	Diaspore	Sulphur	Feldspar	Clino-Pyroxene	Ortho-Pyroxene	Hornblende	Mica
100																														5				
200										4																				12				
300		6																												6				
400										2																				2				
500										3														0.5						7				
600										4														1						2				
700				5						1																				5				
800				1						1															1					6				
900				1																					1					11				
1000				3									0.5											0.5						7				
1110				7									0.5											1						8				
1260				15									0.5											1						14				
1400				6																				0.5						13				
1490				6																				0.5						7				
1600				4									0.5											1	1					7				
1700				26									1																	14				

Table 2-4-4 Results of X-ray Diffraction Analysis of Well AMJ-2

坑井AMJ－2におけるX線回折解析結果

Depth (m)	Alteration Minerals																												Relics				
	I				II	III				IV					V							Others											
	Opal	Tridymite	Cristobaliste	Quartz	Alunite	Halloysite	Kaolinite	Dickite	Pyrophyllite	Smectiete	Chl./Smect.	Mica/Smect.	Chlorite	Sericite	Stiblite	Heulandite	Mordenite	Laumontite	Wairekite	Na-feldspar	K-feldspar	Gypsum	Anhydrite	Calcite	Pyrite	Hemataite	Gibbsite	Epidote	Diaspore	Sulfphur	Feldspar	Clino-Pyroxene	Ortho-Pyroxene	Hornblende	Mica
100			2				1			0.5														1							5				
200			2							2															0.5						5				
300		2	1							0.5														1							7				
400			0.5	5						1																					6				
500			1							2																					13				
600			0.5							4																					14				
700			0.5	5	1					0.5															0.5						6				
800			1	5						0.5														0.5							6				
900			0.5	5			0.5			0.5														1							7				
1000				4			0.5			0.5																					8				
1100			1	9			0.5						1											1							6				
1200				5									1											1	0.5						9				
1300				11									1																		8				
1400				5									1											0.5							6				
1500				8									1											1	0.5						11				
1600				7									0.5											1	0.5						6				
1700				10					0.5				1																		5				

Table 2-4-5 Result of chemical and isotope analyses of hot water samples

熱水試料の化学・同位体分析結果表

NAME	AMJ-1		AMJ-2a		AMJ-2b		AMJ-2c		AMF-2(1998)	
DATE	Nov/25/2000		Nov/27/2000		Nov/28/2000		Nov/29/2000		Oct/22/1998	
W.H.P.(psi)	700		29		33		64		32.7atg	
SAMPLING POINT	silencer muffler		weir box		weir box		weir box		sampling separator	
WATER-TEMP. (℃)	84		90		90		90		<60	
pH(18℃)	7.95		7.57		7.56		7.55		5.25	
EC (μS/cm)	4230		13700		13800		13400		9030	
TSM (mg/L)	3230		9440		9500		9370		6150	
	mg/L	meq/L	mg/L	meq/L	mg/L	meq/L	mg/L	meq/L	mg/L	meq/L
Na	760	33.06	2540	110.48	2520	109.61	2510	109.17	1630	70.90
K	132	3.38	523	13.38	524	13.40	531	13.58	345	8.82
Ca	10.3	0.51	73.3	3.66	72.5	3.62	67.1	3.35	39.1	1.95
Mg	0.071	0.01	0.117	0.01	0.086	0.01	0.071	0.01	0.018	0.00
total cation		36.95		127.52		126.63		126.11		81.67
Cl	1220	34.41	4480	126.35	4500	126.91	4420	124.66	2970	83.76
SO_4	28.2	0.59	39.3	0.82	36.7	0.76	32.6	0.68	11.7	0.24
HCO_3	137	2.25	55	0.90	54	0.88	49	0.80	37	0.61
CO_3	n.d.	0.00	n.d.	0.00	n.d.	0.00		0.00	n.d.	0.00
total anion		37.24		128.07		128.56		126.14		84.61
	mg/L		mg/L		mg/L		mg/L		mg/L	
Li	1.35		19.5		18.7		18.3		9.90	
Fe	0.26		0.50		0.22		0.38		0.16	
Al	0.35		0.38		0.15		0.20		0.58	
Sr	0.14		0.45		0.41		0.37		0.36	
F	0.79		1.98		2.07		1.91		0.49	
B	42.0		75.6		77.1		74.1		45.9	
Br	5.1		17.9		18.1		17.8		10.1	
I	0.74		0.99		0.91		0.96		1.52	
As	3.56		8.69		8.64		8.41		5.39	
Hg	-		<0.0005		<0.0005		<0.0005		0.0009	
$T\text{-}CO_2$	111		134		174		139		68	
H_2S	-		<0.04		<0.04		<0.04		3.76	
$T\text{-}SiO_2$	765		1030		1100		1130		745	
$\delta D(H_2O)$ (‰)	-25		-33		-36		-36		-46	
$\delta^{18}O(H_2O)$ (‰)	1.5		-1.1		-1.3		-1.6		-3.7	
$\delta^{18}O(SO_4)$ (‰)	-		0.8		2.0		2.0		1.1	
$\delta^{34}S(SO_4)$ (‰)	-		10.7		11.5		12.0		15.8	
$\delta^{13}C(HCO_3)$ (‰)	-		-16.9		-22.8		-22.4		-5.2	
Tritium (T.U.)	-		<0.3		<0.3		<0.3		<0.3	
$\delta D(H_2O)^*$ (‰)	-		-42		-42		-43		-	
$\delta^{18}O(H_2O)^*$ (‰)	-		-2.3		-2.3		-2.5		-	
NOTE									separated from steam at 0.8atg	

n.d.: not determined

*: sampled at sampling separator

Table 2-4-6 Result of chemical and isotope analyses of gas samples

ガス試料の化学・同位体分析結果表

NAME		AMJ-1a	AMJ-1b	AMJ-1c	AMJ-2a	AMJ-2b	AMJ-2c	AMF-2(1998)
DATE		Nov/19/2000	Nov/20/2000	Nov/21/2000	Nov/27/2000	Nov/28/2000	Nov/29/2000	Oct/22/1998
W.H.P.	psi	200	110	46	29	33	64	32.7atg
SAMPLING POINT		sampling separator	sampling separator	sampling separator	sampling separator	sampling separator	sampling separator	sampling separator
SEPARATED PRESSURE	barG	2.4	1.3	1.4	0.5	0.7	0.5	0.8atg
GAS CONTENT	vol%	0.98	1.02	0.97	0.52	0.62	0.58	0.84
GAS CONTENT	wt%	2.28	2.41	2.29	1.22	1.46	1.36	2.01
GAS COMPOSITION								
CO_2	vol%	89.9	93.8	92.5	88.3	90.6	87.6	96.8
H_2S	vol%	2.80	3.90	5.30	9.30	6.90	10.1	2.01
Residual gas	vol%	7.3	2.4	2.2	2.4	2.5	2.3	1.2
RESIDUAL GAS COMPOSITION								
N_2	vol%	75.3	59.8	53.4	73.0	68.1	64.8	71.1
H_2	vol%	n.d.	n.d.	7.44	8.46	12.5	13.9	17.8
CH_4	vol%	7.42	35.5	34.3	12.3	11.7	11.0	8.67
C_2H_6	vol%	-	-	-	-	-	-	0.37
O_2	vol%	16.4	3.94	4.22	5.32	6.80	9.18	1.68
Ar	vol%	0.84	0.78	0.58	0.92	0.80	1.07	0.34
He	vol%	0.0072	0.021	0.023	0.019	0.019	0.018	0.053
Ne	vol%	0.0015	0.00074	0.00051	0.0012	0.00080	0.0027	0.0007
$^3He/^4He$	$\times10^{-6}$	10.37±0.13	10.31±0.14	10.45±0.15	10.46±0.14	10.52±0.12	10.44±0.09	10.64±0.09
$^4He/^{20}Ne$		44	18	68	21	23	23	123
$\delta^{13}C(CO_2)$	‰	-6.8	-8.4	-7.4	-6.8	-6.9	-5.9	-3.0
$\delta^{13}C(CH_4)$	‰	-30.5	-30.4	-30.4	-27.4	-27.6	-26.5	-33.1
$\delta D(H_2)$	‰	n.d.	n.d.	-379	n.d.	-409	-493	-485
$\delta D(CH_4)$	‰	-208	-221	-227	-196	-205	-187	-227
$\delta^{34}S(H_2S)$	‰	2.5	1.6	1.0	1.4	1.4	1.4	n.d.
CONDENSED WATER CHEMISTRY								
pH	20℃	6.20	5.85	5.66	5.03	5.03	5.00	-
Na	mg/L	0.902	0.408	0.402	0.380	0.093	0.112	-
Cl	mg/L	1.20	0.54	0.56	0.64	0.12	0.16	-
SO_4	mg/L	1.5	1.2	0.8	1.3	0.8	1.3	-
As	mg/L	0.014	0.013	0.012	0.006	0.031	0.016	-
Hg	mg/L	0.0009	0.0011	<0.0005	<0.0005	<0.0005	<0.0005	-
$\delta D(H_2O)$	‰	-56	-55	-54	-59	-59	-60	-67
$\delta^{18}O(H_2O)$	‰	-3.8	-3.4	-3.3	-6.1	-6.1	-6.6	-7.7

n.d.: not determined due to low concentration of CH_4, H_2 and H_2S

Table 2-4-7 Specifications of borehole surveys for well AMJ-1 and AMJ-2

坑井 AMJ-1 および AMJ-2 の温度・圧力検層の仕様

Concept	Analysis Method	Objectives	Specifications
Static pressure and temperature surveys **Stops for surveys to Casing shoe (CS) depth** Every 50m of 10 min each. Two stops should be 15m to be used as markers in the recording charts **Stops for surveys to total depth (TD)** Up to casing shoe, stops every 100m. From CS to TD, every 50m of 10 min each. Additional stops of 10 min. At total loss depths,. 15 min stops at 1100m and 1500m to be used as markers in the recording charts	Visual interpretation Statistical regression Analysis on temperature data	Guidance to set casings Estimation of formations temperature Reservoir pressure.	**CS depth surveys** Set of three (5h, 12h and 24h) P/T surveys before cementing the 9 5/8" CSG. **From CS to TD depth:** Blind Drilling - Drill 100 more after total loss - Run a set of three (5h, 12h and 24h) P/T surveys - Run a set of four (5h, 12h, 24h and 48h) P/T surveys at total depth **Normal Drilling** - Run a set of four (5h, 12h, 24h and 48h) P/T surveys at total depth **Logistic** Field logistic and measurements done using INDE's tools and crew. Support by Driller

Table 2-4-8 Specifications of Water loss temperature test in AMJ-1
坑井 AMJ-1 の逸水量確認試験要領

Concept	Analysis Method	Deliveries	Specifications
Static pressure and temperature surveys while injecting water **Remarks** 1. The capacity of the water tank was 240m^3 and of the mud tank was 120m^3 , therefore, there was a total water storing capacity of 360m^3 . 2. This capacity represents 20 hours of testing when injecting 30 m^3 /h (360m^3/ (30.-12.5) m^3/h) which will be enough to suppress conduction effects. 3. 19 stops in total; from 800m to 1400 10 min. stops every 100mat intervals. From 1400m to 1680m 10 minutes stops at intervals of 20 m. At 1500m and 1600m the stops were 15min. long. The total testing time was 3.25 hours. The total water used was be 100.5 m^3 and the water in tanks was be 300 m^3 (360-100.5+12.5*3.25). The time required to refill the tanks will was 4.8 hours.	Visual interpretation	Estimation of positions of feed points and its relative injection capacity	**Water Injection** Select the minimum flow rate available from the rig pumps or set to 30 T/H. **P/T surveys** Run P/T instruments in the hole 30 minutes after initiating injection to allow for transients to be over. **Stops** 19 stops in total; from 800m to 1400 10 min. stops every 100mat intervals. From 1400m to 1680m 10 minutes stops at intervals of 20 m. At 1500m and 1600m the stops were 15min. long. **Pressure toll** Pressure tool was be run with the temperature tool to utilize the pressure readings in the analysis of the injection tests **Logistic** Field logistic and measurements done using INDE's tools and crew. Support by Simmons

Table 2-4-9 Specifications of Water loss temperature test in AMJ-2
坑井 AMJ-2 の逸水量確認試験要領

Survey	Analysis Method	Deliveries	Specifications
Static pressure and temperature surveys while injecting water **Remarks** 1. 20.0 m^3 /h of water supply capacity. Water pumping capacity 120.0 m^3 /h. Storage in the water tank is 50m^3 and that of the mud tank is 150m^3, therefore, there is a total water storing capacity of 200m^3. 2. This capacity represents 13 hours of testing when injecting 35 m^3 /h (200m^3/ (35.-20.0) m^3/h) which will be enough to suppress conduction effects. 3. The total water to be used will be 140 m^3 and the remaining water in tanks will be 140 m^3 (200-35*4+20*4). The time required to refill the tanks will be 3.0 hours.	Visual interpretation	Estimation of positions of feed points and its relative injection capacity	**Water Injection** Select the minimum flow rate available from the rig pumps or set to 35 T/H. **P/T surveys** Run P/T instruments in the hole 30 minutes after initiating injection to allow for transients to be over. **Stops** 19 stops in total; from 1000m to 1400 10 min. stops every 100m at intervals. From 1400m to 1700m 10 minutes stops at intervals of 20 m. At 1500m and 1600m the stops should be 15min. long. Total test time 4.0 hr. **Pressure tool** Pressure and temperature tools will be run together to get pressure readings for the injection tests **Logistic** Field logistic and measurements by INDE's tools and crew. Support by PITSA

Table 2-4-10 Specifications of Injection and Transient Tests for well AMJ-1
坑井 AMJ-1 の坑井試験要領

Concept	Analysis method	Deliveries	Specifications
Multi Rate Injection Test.	- visual interpretation - Plotting and linear regression analysis	- Injectivity Index.	**Flow rates** 30, 50 and 70 m^3/h during one our each. **Instruments** Pressure elements with 8 hr and 12 hr clock each. **Setting depth** 1600m **Others** Field logistic and measurements done using INDE's tools and crew.
Fall-off Test	- Visual interpretation - Horner Semilog plot - Curve matching analysis	- Storativity (φch) - Flow capacity (kh) - Skin factor - Wellbore storage	**Duration** 3 hours after terminating the last injection rate **Others** Field logistic and measurements done using INDE's tools and crew.

Table 2-4-11 Specifications of Injection and Transient Tests for well AMJ-2
坑井 AMJ-2 の坑井試験要領

Concept	Analysis method	Deliveries	Specifications
Multi Rate Injection Test.	- visual interpretation - Plotting and linear regression analysis	- Injectivity Index.	**Flow rates** 62, 82, 112 and 127 m^3/h during 15, 30, 30, 15 min respectively **Instruments** Pruett capillary tubing and MiniMax **Setting depth** 900m **Others** Field logistic and measurements done using INDE's tools and crew.
Fall-off Test	- Visual interpretation - Horner Semilog plot - Curve matching analysis	- Storativity (φch) - Flow capacity (kh) - Skin factor - Wellbore storage	**Duration** 15 hours after terminating the last injection rate Readings, set automatically to every 8 min. **Others** Field logistic and measurements done using INDE's tools and crew.

Table 2-4-12 Results of the curve matching and hydraulic properties for well AMJ-1

坑井 AMJ-1 の坑井試験結果

kh/MU	4.54E-10	m3/Pa.s	Phi*c*h	1.09E-04	m/Pa	Skin Factor	0.9		WB Storage	30	
kh	4.59E-14	m3	kh	4.59E+01	mdarcy-m	Viscosity	0.0001011	Pa.s	Spec. Vol	0.00101	m3/kg
k	2.53E-16	m2	Phi*Ct	6.003E-07	1/Pa	Stabilization Temp. 1600m	264.53	C	Injection Temp.	25	C
h	1.82E+02	M									

Table 2-4-13 Results of the curve matching and hydraulic properties for well AMJ-2

坑井 AMJ-2 の坑井試験結果

TR=kh/MU	2.84E-09	m3/Pa.s	STO=Phi*c*h	5.85E-06	m/Pa	Skin Factor	-0.5		WB Storage	0	
kh	5.52E-14	m3	kh	5.39E+01	mdarcy-m	Viscosity	1.943E-05	Pa.s	Spec. Vol	0.001013	m3/kg
k	5.66E-15	m2	Phi*Ct	6.003E-07	1/Pa	Stabilization Temp. 1600m	279.28	C	Injection Temp.	50	C
h	9.75E+00	M									

Table 2-4-14 Pre-heating up, stimulation and well testing

噴出試験要領

Concept	Analysis method	Deliveries	Remarks
Warming up	- Visual interpretation - Bleed the well	- Build up WH pressure - Warm up the upper casing - Initial discharge w/o mechanical stimulation	Field logistic and measurements done using INDE's tools and crew.
Stimulation	- Visual interpretation - Bleed the well - Compress the water level	- First discharge and cleaning the borehole of mud water	Self pressure build up or connection to other production well or use of Driltech's compressor
Flow Tests.	- Lip Pressure and Weir Method	- Steam and water mass flow at WH conditions. - Production enthalpy at WH conditions. - Production characteristic curve	Field logistic and measurements done using INDE's tools and crew. - Foundation construction - Silencers - Weir - Level meter - Discharge pipes - Orifices - Manometers - Differential pressure manometers - Barton recorders - Tools - Spare parts

Table 2-4-15 Specification for the dynamic pressure, temperature surveys

噴出時の坑内検層要領

Survey	Analysis Method	Objectives	Specifications
Dynamic pressure, temperature and spinner surveys	Visual interpretation Wellbore simulation	Disclose relative productivity of the different feed points Estimation of feed points enthalpies Estimation of the feed point production.	**Up to 1000m depth surveys** One P/T/S survey after the second day of discharge at full open valve or when stable lip pressure readings are recorded **Assembly** Assemble pressure tool temperature tool and spinner tool with sinker bar of enough weight to stand the drag force of the ascending fluid. **Stops for surveys to total depth** Up to 1000 m, stops of 10 minutes every 100m. From 1000 to 1700m, every 50m stops of 10 min each. 15 min stops at 1200m and 1600m to be used as markers in the recording charts **Logistic** Field logistic and measurements done using INDE's tools and crew. S

2.5 Geothermal Conceptual Model

2.5.1 Geological Structure

2.5.2 Heat Source

2.5.3 Temperature Distribution

2.5.4 Geochemical Model

2.5.5 Conceptual Model

2.5 GEOTHERMAL CONCEPTUAL MODEL

From geo-scientific surveys such as geological reconnaissance, geochemical and geophysical survey, and various well surveys, the geothermal conceptual model in the Amatitlan area was prepared and updated.

The geological result allowed the identification of the basement structure, faults system and the dacitic intrusion controlling the geothermal activity present in the Amatitlan field. In addition, the comprehensive analysis of rock age and hydrothermal alteration permitted the disclosure of the volcanic activity associated to the heat source and to the geothermal activity of the area.

In addition to review the chemistry of thermal springs and the fumarolic activity, the geochemical analysis for geothermal fluids from wells AMJ-1 and AMF-2 permitted the estimation on the up-flow pathways, the characteristics and the pattern of geothermal fluids. Finally a geochemical model was constructed.

The uplifted zone of basement, the altered area, the extent of geothermal reservoir and resistivity structure was estimated from the gravity, magnetic and MT survey. This information were compared and reviewed with the result of well survey (shown to Fig.2-5-1, Fig.2-5-2 and Fig.2-5-3).

2.5.1 Geological structure

An uplift zone related to faults in N-S and NE-SW direction, by a system of calderas and by a dacitic intrusion characterizes the geological structure in the Amatitlan geothermal field.

1. Uplift Zone related to Faults in N-S and NE-SW Direction

N-S trending uplift zone of 1.5 – 2.0 km width was estimated in the center of the surveyed area from the results of the geological and gravity surveys.

This uplift zone is partly bent in NE-SW direction between Cerro Hoja de Queso and well AMF–2. Water loss circulation at the depth of 1594m in well AMJ-2 may correspond to the fault associated to the west edge of this uplift zone. At this depth, reservoir temperature over 280°C was confirmed by logging conducted in wells AMF–1 and AMF–2. The extension and distribution of fumaroles and alteration zones are parallel to this uplift zone. As shown to Fig.2-5-3, dacite intrusion occurs along the fracture zone along the west end of this uplifted zone. A part of this intrusion was confirmed by the cuttings analysis of well AMF-2.

It was confirmed by drilling of wells AMF–1 and AMF-4 that basement rock forms a relative upheaval at an altitude of 400 – 500 m compared than the low elevation, about 230m in altitude, of well AMJ-1 basement. Generally, the uplift zone of poorly permeable granite basement is likely to correspond to the upflow zone of geothermal fluids in typical geothermal fields.

2. A System of Calderas

INSIVUMEH (1978), OLADE (1982) AND Roldan (1993) report to exist three delineated calderas around the study area. The geothermal activity in Amatitlan area is considered to be associated to the southern rims of these calderas. These calderas rims are traced from the following faults-systems

(Fig.2-5-1):

a. An outermost caldera

The outer and oldest caldera is passing beneath Cerro Grande and north Cerro Chino and reaches to east Volcan de Agua through the valley along Rio Michatoya. The meteoric water may infiltrate into at the shallow zone in the study area due to no geothermal features along caldera lineation on the surface.

b. A middle caldera

The second oldest caldera forms the wall facing southeast shore of Lago de Amatitlan. Between well AMJ-1 and AMJ-2, through EL Cedro and San Vicente Pacaya, the caldera outline ends up to Jalpatagua fault. Water loss circulation around 1,140m depth of well AMJ-2 may correspond to the fault associated to this caldera rim.

The MT survey shows the low resistivity zone with NW-SE extension near wells AMJ-1, AMJ-2, AMF-2 and El Cedro. In addition, as mentioned below, the high anomaly of temperature distribution bent toward northwest direction along middle caldera rim. The fact indicates that fractured zone developed along this middle caldera is highly permeable.

c. An innermost caldera

This caldera is estimated as the youngest one from the previous reports and passes through Cerro Hoja de Queso, near well AMF-4 and north San Vicente Pacaya. Since water loss circulation was reported around 1,000m depth of well AMF-4, the cold water might percolate along faults and fractures associated to this youngest caldera rim. In contrast, the low temperature zone extends over at the northeastern part of the study area. This suggests that Lago de Amatitlan water is supposed to infiltrate along the permeable zone relevant to this caldera rim.

In addition, a relatively small caldera, Luguna Caldera, was recognized at the west of Laguna de Calderas. Water loss circulation around 1,539m depth of well AMJ-2 may result from the fault associated to the rim of Luguna Caldera. Since the extension and distribution of fumaroles and alteration zones are similar to the shape of this caldera rim, this caldera rim is anticipated to be the up-flow zone of high temperature fluids from the greater depth.

3. Intrusion of Dacite

Dacite intrusion was confirmed to exist around well AMF-2 by well geology. Since this intrusion is similar to the dacitic domes near south shore of Lago de Amatitlan in petrological characteristics and age, it was pointed out that this intrusive activity certainly happens at the same age of dome formation (West JEC and Telectro, 1995). It is possible that these intrusion bodies are distributed along the west side of the uplift zone estimated by gravity survey beneath Laguna Caldera (Fig.2-5-2 and Fig.2-5-3).

According to fluid inclusion analysis of cuttings, the homogenization temperature shows the bimodal distribution below 1,100m depth of wells AMJ-2, AMF-1 and AMF-2. It is thought that the deeper portion around

these wells may be reheated and the temperature increased by newly activated hydrothermal events.

In other words, when the dacitic magma rose and shaped the intrusion, the fracture zone developed around the intrusion and then possibly becomes a path of geothermal fluid flow.

2.5.2 Heat source

It is obvious from the result of age determination that the center of the volcanic activities has migrated from north to south in Amatitlan area. It is recognized that the hydrothermal activity also has migrated in the same direction. This series of volcanic activities continues from the late Pleistocene (0.7Ma) to present. The regional heat source for Amatitlan geothermal system is interpreted and associated to a series of this magmatism, including recent activities of Volcan de Pacaya, which was erupted on January 17, 2000, with large scaled Strombolian type.

We attempted to identify the direct heat source for Amatitlan geothermal system on the basis of well surveys, geological structure, age determination, temperature distribution described below, geochemical fluid characteristics, etc.

a. As shown in Fig. 2-5-2 and Fig.2-5-3, the temperature above 300℃ is expected at the top of the basement consisting of granite porphyry.

b. From the observation of cuttings and their zircon crystal forms, dacitic rocks of AMJ-1, AMJ-2 and AMF-2 are similar to those of Dacite domes adjacent to Lago de Amatitlan. Especially, Dacite tapped at 560-870m depth of AMF-2 is estimated to compose of a part of the intrusion. In addition, this intrusion is thought to have activated in the same age, 3-6ka, when Dacite dooms was shaped at Cerro Limon and Cerro Duranzo.

c. The homogenization temperature of fluid inclusions shows a bimodal distribution below 1,100m depth of well AMJ-2, as well as AMF-1 and AMF-2. This may indicate about 50℃ increase due to the newly intruded Dacite. This kind of temperature increase is not confirmed on other wells.

d. From the temperature distribution, as mentioned later, the high temperature anomaly in the study area is found around from wells AMJ-2, AMF-1 and AMF-2. The shape of this anomaly area is quite harmonious with that of Laguna Calderas rim.

From the above interpretations, it is estimated that the dacitic magma intruded along faults related to west edge of the basement upheaval zone and to caldera rim in the age of 3-6 ka and the dacite rock body exists inside Laguna Caldera. Furthermore, it is highly possible that this dacite body itself plays a role of the direct heat sources in Amatitlan geothermal system.

2.5.3 Temperature Distribution

The temperature distribution map was made on the basis of logging data and homogenization temperature of fluid inclusions from 6 wells drilled in the survey area.

a. The highest temperature in the study area is observed around the bottom of well AMF-2. The temperature above 300°C was confirmed around the top of the basement consisting of granite porphyry. At the altitude of 200m, the maximum temperature of 320°C was recorded by logging measurement.

b. The reversal phenomenon of underground temperature appears near 500m altitude of well AMF-3 and a isothermal line of 200°C at same elevation extends towards the north in the tongue shape (refer to Fig.2-5-3). This fact suggests that high temperature fluid flows laterally toward the north along the uplifted basement zone.

c. The isothermal line is bent toward the northwest from the surrounding area of well AMJ-1. Low resistivity area indicated by MT survey has a harmonious elongation along the middle caldera rim. According to the geochemical analysis, lateral flow of high temperature fluid was reported to reach to Rio Michatoya in same direction. From these evidences, the fractured zone developed along this middle caldera is highly permeable and plays a role of fluid passage.

d. Around well AMF-4, slight anomaly of relatively low temperature extends in ESE direction. Meteoric water or underground cold water at shallow portion of this well may percolate along fault associated to the innermost caldera rim. This estimation is harmonious to the depth of water loss circulation encountered around 1,000m depth of well AMF-4.

In conclusion, underground temperature in the study area has a center around the dacite intrusion body beneath the westward of Laguna de Calderas and decreases concentrically. The temperature distribution has, in general, an appearance with fluid flow reflected geological structure relevant to the uplifted basement structure and a series of caldera rims.

2.5.4 Geochemical Model

Based on the geochemical interpretation regarding the reservoir fluids, the geochemical model of the Amatitlán geothermal field was reconstructed (Fig.2-5-4).

The geothermal reservoirs tapped by the wells AMJ-1, AMJ-2, AMF-1 and AMF-2 may compose a single hydrothermal system. Although the discharge fluid from the wells is only steam at the AMJ-1 and including excess steam at the AMJ-2 and AMF-2, the system is essentially a liquid dominated. All of these reservoir fluids are possibly derived from a common parent fluid of ca.330°C and ca.2,500mg/L in Cl. The origin of the reservoir fluid is basically considered to be deep circulated meteoric water with minor magmatic fluid. The meteoric water is possibly a mixture of high altitude precipitation of the south side and low altitude water from north and northeast sides including the lake water of Lago de Amatitlán. According to Cl/B ratios in discharged water, the main reservoir host rock is believed to be volcanic rocks and not the basement granite.

The main upwelling zone is thought to be close to the wells AMF-2 and AMJ-2, since the highest fluid temperature (290-300 °C) is estimated by the geothermometries for these wells. The ascent of the deep hot fluid is likely

accompanied by partial boiling, providing the reservoir fluids slightly higher in Cl (ca.2,700mg/L) than the parent fluid. Further boiling during the fluid ascent may produce the fluid fed at the shallower depth of the well AMJ-2, which is relatively cool (<280℃) and relatively high in steam fraction and in Cl (>2,800mg/L). Possibly larger part of the high temperature fluid flows laterally northeastward with further boiling and steam separation, producing the reservoir of the well AMF-1. A part of the steam separated from the fluid ascends to shallow part to make the fumaroles at Calderas. The fluid at the reservoir of the well AMF-1 is affected more by the steam separation which yields temperature decline to around 250℃ and enrichment of Cl up to around 3,300mg/L. The fluid ascended at Calderas flows laterally toward mainly north and northeast directions with dilution by cool groundwater, and finally discharges at the south shore of Lago de Amatitlán.

Although the fluid in the geothermal reservoir of the well AMJ-1 is thought to originate from the parent fluid, the pathway of the fluid being supplied to the reservoir is unclear. However, according to the chemical monitoring of the well AMF-1 and AMF-2, the AMJ-1 reservoir, at least, has some connection with other ones. The reservoir fluid seems to be significantly vaporized due to the low permeability. The gas geothermometries indicate the reservoir temperature of 260-280℃.

Though it is not depicted in the model of Fig.2-5-4, as mentioned in the previous studies, the outflow of the high temperature fluid toward west reaching Rio Michatoya valley may exists, providing many hot springs with mixing with shallow ground water at the valley.

2.5.5 Conceptual model

The model of geothermal system in the Amatitlan area is considered to be hydrothermal convection system resulted from meteoric water originated in southern highland and Lago de Amatitlan (shown in Fig.2-5-1, Fig.2-5-2, and Fig.2-5-3). This system is thought to be directly heated by dacitic intrusion beneath the westward of Laguna de Calderas and is regionally affected to upflowing heat and gases from the remained magma after the volcanism continuing from Late Pleistocene (0.7Ma) to Recent, such as dacitic domes, the intrusion, repeated eruption of Volcan de Pacaya, etc.

Recharged meteoric water is considered to flow toward the north or the northeast upon the granitic basement rocks. The flowing meteoric water is heated by conductive heat from the remained magma and changes to neutral chloride type hot water by interaction with surrounding rocks. This hot water contains upflowing gases from basement rocks and rises up to 300-340℃. This deep water is supposed to be parental fluid in the Amatitlan geothermal systems.

The ascent of the deep hot fluid is reserved mainly along faults related to west edge of the NE-SW trending basement upheaval, faults formed Laguna Caldera rim at the west of Laguna de Calderas, and fracture zone developed around the intrusion by the dacitic magma rise.

At the altitude of 500m beneath well AMF-2, the geothermal fluid is 290-300℃ in temperature and 2,700mg/l in Cl content. This hot fluid is vertically flowing up through the NE-SW trending fault and yields fumaroles and altered zones at the

west-wall of Laguna Caldera. Horizontally, this fluid reaches to well AMF-1 along the NE-SW fault under boiling and yields to the water-dominated reservoir with relatively low enthalpy and high salinity tapped by this well.

Boiling accompanied with the upflow of geothermal fluids results in silica depreciation and hydrothermal alteration in the shallow part. It leads to form the cap-rock in the geothermal reservoir. This hydrothermal alteration portion was identified by the MT measurements as a low resistivity anomaly. In the area beneath and surrounding wells AMF-1 and AMF-2, there is a two-phase reservoir coexisting steam and liquid just below this cap-rock. From the distribution of this low resistivity anomaly, the hydrothermal alteration portion possibly extends towards the north with a banded-shape. Geochemical analysis suggests that the hot water is gradually diluted by meteoric water during its travel towards the north. Finally, the temperature decreases and it forms the hot spring aquifer adjacent to the shore of Lago de Amatitlan.

On the contrary, it seems that the cap-rock will be with difficulty extend toward the west due to the less development of the alteration zone around wells AMJ-1 and AMJ-2.

The phenomenon of temperature decline downward was recognized at well AMF-3. This suggests that the Lago de Amatitlan water may be percolating at elevation between 0-500m towards the southwest and be cooling the underground temperature at the northeastern part of the study area.

Dacite intrusion beneath the eastward of well AMF-2 is similar to dacite domes adjacent to Lago de Amatitlan in the zircon crystal form and the geological age. The fact is in high possibility that dacitic magma intruded in the same age (3-6ka) as dacite domes were formed at Cerro Limon and Cerro Duranzno.

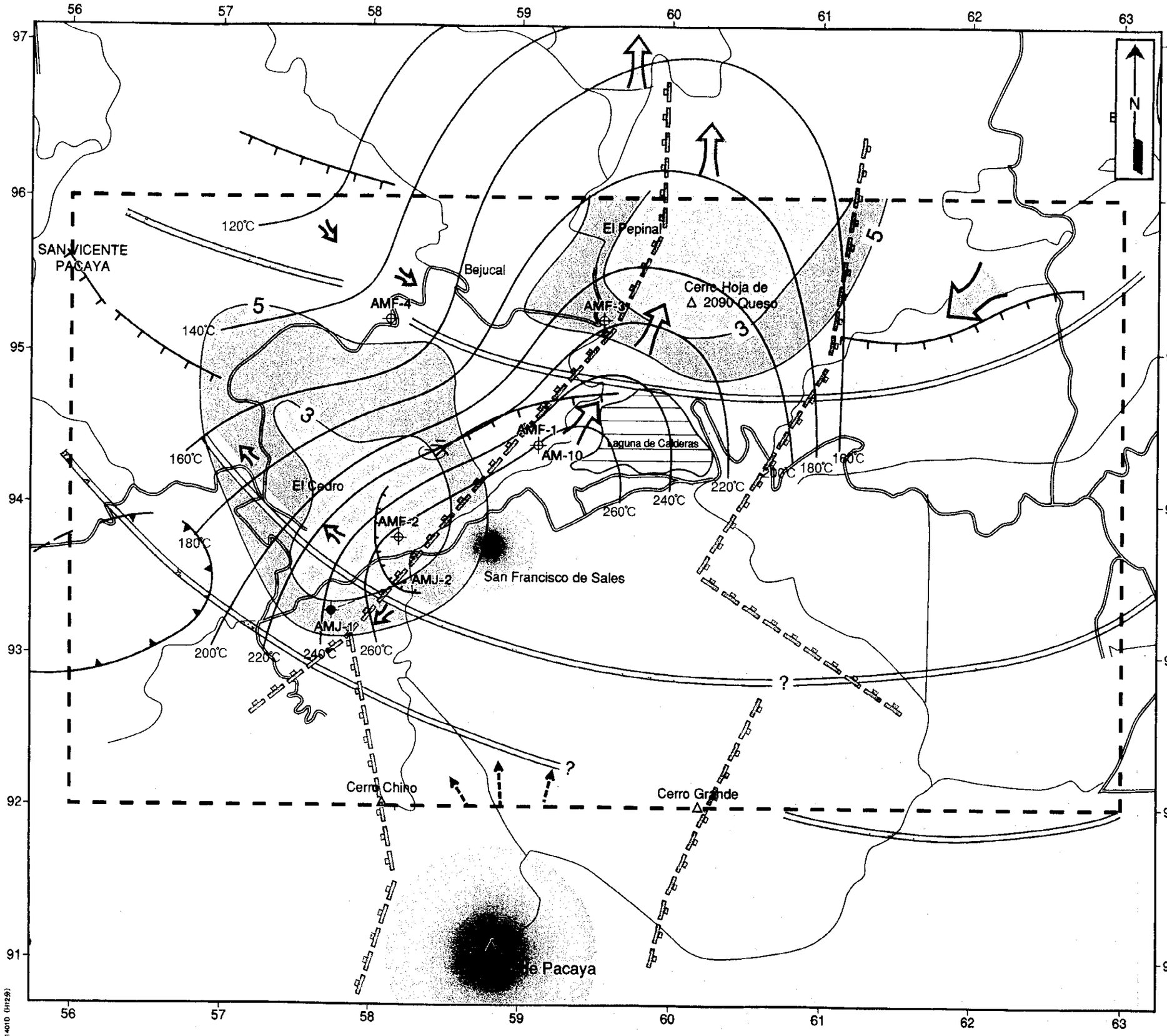

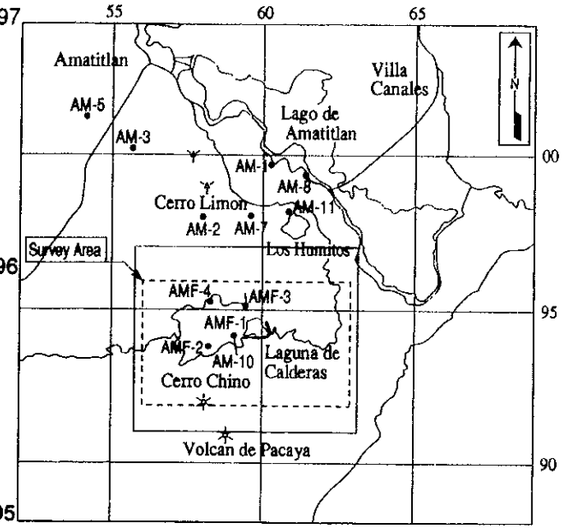

凡 例

- Estimated uplift obtained from gravity survey
- Phreatic Caldera and abalanche
- (Estimated) Fault
- Caldera Wall
- Low resistivity zone
- 280℃ Isothermal Line (EL.+750m)
- Magmatic fluid
- Geothermal fluid
- Meteoric water flow
- Survey area
- Exploratory well
- (Estimated) Heat Source

1:25,000

1 1/2 0 1km

Amatitlan Geothermal Development Project	
地熱構造モデル（平面図）	
Geothermal Structual Model	
JICA-WEST JEC	Fig. 2-5-1

M98101401D (H12分)

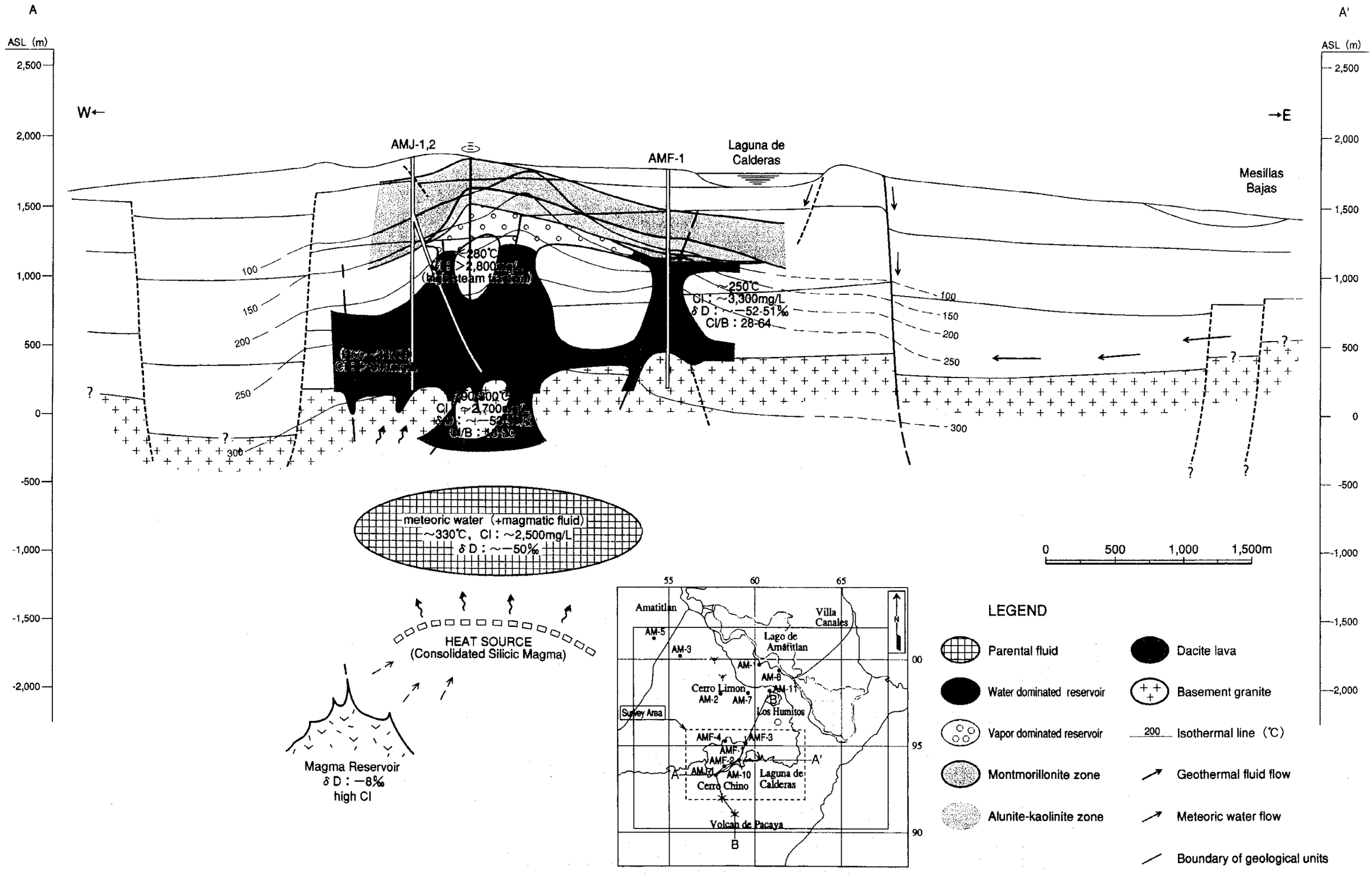

Fig. 2-5-2 Conceptual model of the Amatitlan Geothermal Area (A-A')
地熱構造モデル（A-A'断面図）

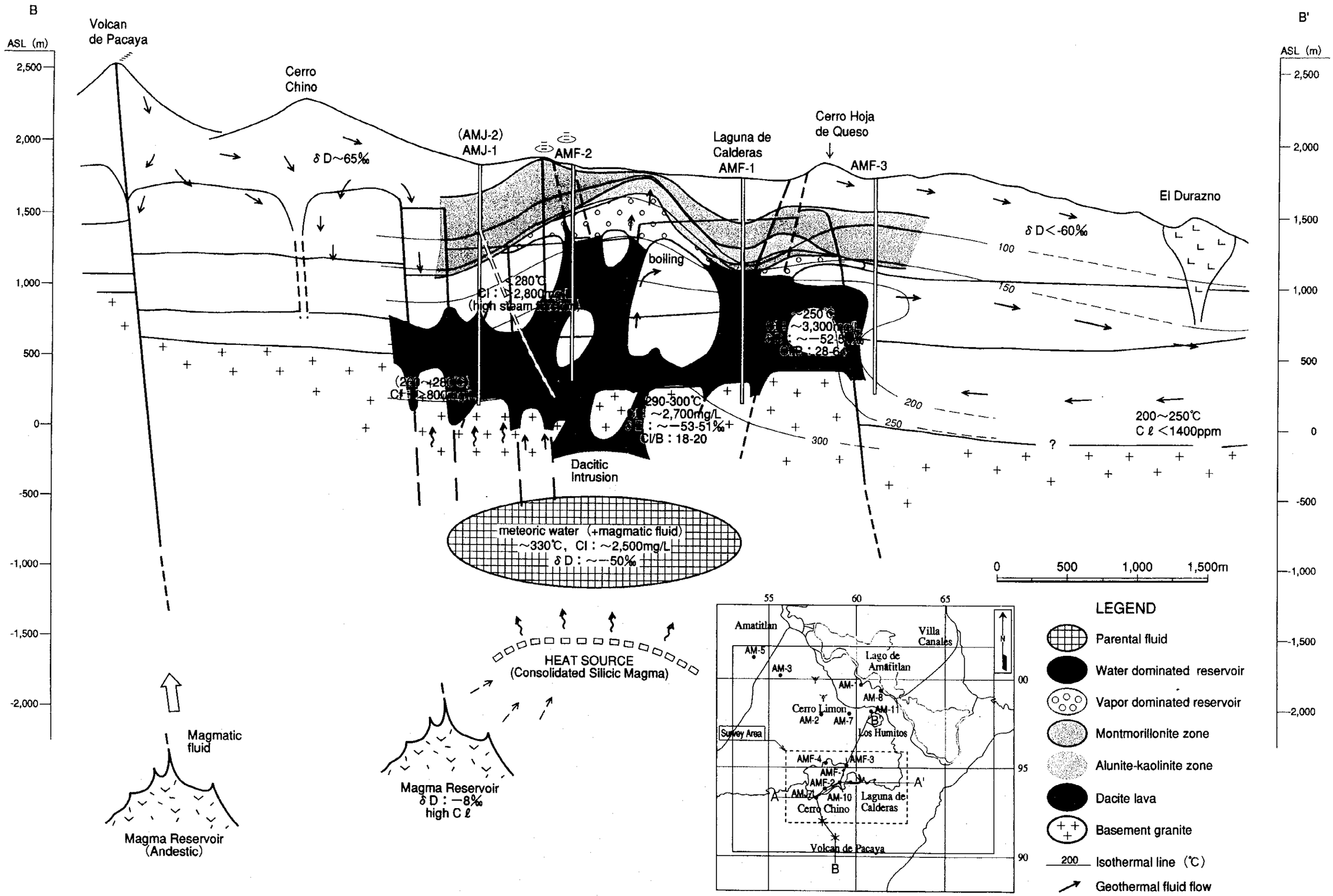

Fig. 2-5-3 Conceptual model of the Amatitlan Geothermal Area (B-B')
地熱構造モデル（B-B'断面図）

M88101401D (H12-9)

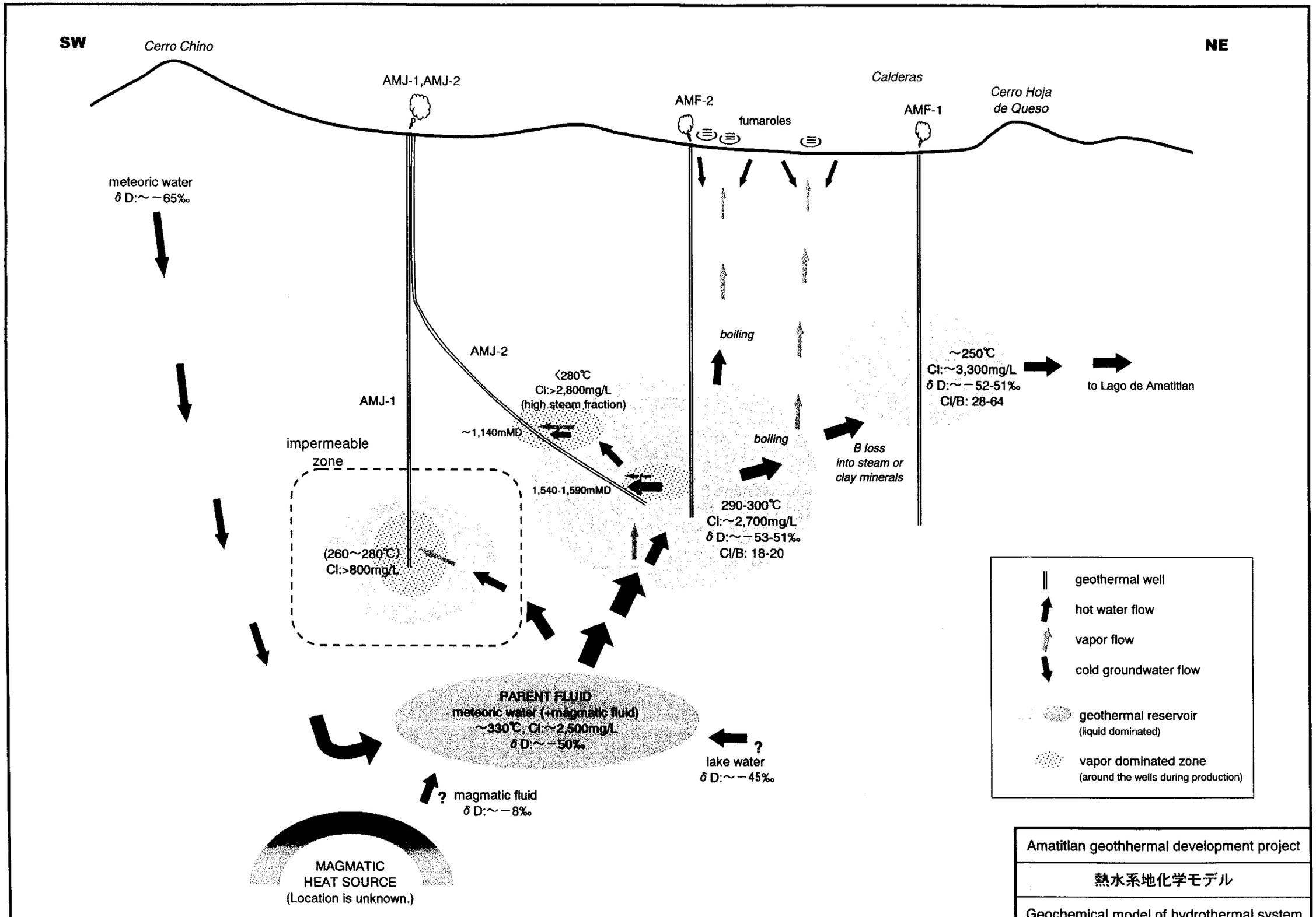

Amatitlan geothhermal development project	
熱水系地化学モデル	
Geochemical model of hydrothermal system	
JICA-WEST JEC	Fig. 2-5-4

3 DEVELOPMENT PROGRAM

3.1 Resource Assessment

3.2 Development Plan of Power Plant

3.3 Envionmental Impact Assessment

3.4 Economical and Financial Evaluation

3.1 Resource Assessment

3.1.1 Numerical Model

3.1.2 Natural State Calibration

3.1.3 History Matching Calibration

3.1.4 Forecasting and Field Potential

3.1.5 Results of Forecasting

3. DEVELOPMENT PROGRAM

3.1 RESOURCE ASSESSMENT

Detailed explanation of the process and results of natural state and history matching calibrations can be found in the Interim report to JICA of March 2001. Hereafter a summary of these topics is given. In the same report to JICA a forecasting of the reservoir response to exploitation is described with the objective of estimating the power potential of the reservoir. Here, a more detailed assessment is done in order to comply with the Term of Reference of JICA for the Fiscal Year 2001.

3.1.1 Numerical Model

To proceed to the potential estimation and to the simulation of the Amatitlan reservoir, a procedure shown in Fig. 3-1-1 was applied. The control volume was selected as shown in Fig. 3-1-2. The simulation model was oriented in a NS - EW direction. The model includes a total area of 140 km^2 (14 km in the NS direction and 10 km in the EW direction), much larger than the known geothermal area. The large area was required, however, to ensure a reasonable representation of the overall geological framework of the geothermal system and to reduce the effects of the boundary conditions on the simulation model.

Five different layers were devised to represent the reservoir in the "z" (depth) direction. Fig. 3-1-3 shows this five layers.

The configuration of the grid in the different layers had to be different to represent the features of the geothermal system. Layer 1 (AE) and Layer 4 (AB) have the same configuration with 225 elements each. Layer 2 (AD) and Layer 3 (AC) have the same configuration with 285 elements each and Layer 5 (AA) has 190 elements. In total there are 1210 elements in the control volume.

In addition, boundary blocks were set beneath Layer 5 (AA) to represent the portions of the conceptual model supplying hot fluids to the system and boundary blocks above layer 1 (AE) to represent air and the topography of the Amatitlan field. To represent the lateral supply of water from the regional hydrological system Layer 2 (AC) was added in boundary blocks.

Table 3-1-1 presents the values of the petrophysical properties of materials filling the several elements of the numerical model.

The initial permeability distribution was based on available results from well test analyses. These values were modified during the initial state modeling to obtain the sub-surface temperature matches. Porosity was assumed to be constant at a value of 5% throughout the model, which is typical for a two-phase, high temperature reservoir. Thermal conductivity of the water-saturated rocks in the reservoir was assigned a constant value of 2.2 W/m.°C. Two specific heat numbers were used in the model; 1000 kJ/kg.°C for active blocks and 50,000 kJ/kg.°C for boundary blocks. The high value of specific heat is used as a "flag" in the model to exclude those blocks from mass and energy balance calculations. The relative permeabilities were specified in the model using "X" type curves, with zero residuals for steam and water.

The definition of the model was completed when boundary blocks were specified

to define the heat and mass inflow and outflow from the model. The boundary blocks include:

1. One that is attached to the bottom layer (layer 5) of the model to provide for conductive heat transfer to/from the model from below;

2. One that is attached to six gridblocks of the bottom layer (layer 5) just north of Pacaya Volcano to supply heat and mass recharge to the model;

3. Three that are attached to three blocks on the N side of layer 1 to allow for shallow discharge towards Lake Amatitlán, including the hotsprings and fumaroles located along the shoreline;

4. One discharge block that is attached to a block of layer 1, west of well AMF-2 to represent shallow discharge in this direction including the fumaroles in this area;

5. One attached to ten gridblocks at the NE corner of layer 3 providing cool fluid to the model to simulate the deep regional (NE to SW) fluid flow pattern;

6. One that is attached to three gridblocks at the SW side of layer 3 to allow deep subsurface discharge towards the Michatoya River.

7. One that is attached to the southern portion of the model to allow conductive heat loss to the overlaying terrain in this area, and;

8. A final boundary block that represent the atmosphere above the model and allows for conductive heat loss to a constant atmospheric temperature of 30° C

3.1.2 Natural state calibration

The main objective of the natural state calibration was to verify the temperature and pressure distributions and the heat/mass flow aspects of the model. In this context, the major rock properties of importance were permeability and thermal conductivity. Unlike forecasting modeling, storage related parameters such as porosity, density and specific heat of the rock are not important initial state modeling parameters. Therefore in initial state modeling it generally suffices to use average values of porosity, density and specific heat of the rock, but more detailed distributions need to be specified for permeability and thermal conductivity of the rock in order to match the sub-surface temperature distribution.

As with most geothermal systems, heat and mass recharge and discharge must be present in order to maintain the thermodynamic equilibrium within the reservoir. As mentioned above, the model includes two recharge sources and five discharge sinks that were introduced in order to match the subsurface temperature data. A hot inflow rate of about 450 tons/hour was required into the six blocks in layer 5; the inflowing fluid is single-phase water at a source temperature of 336°C. An additional inflowing fluid at 50°C is coming from the NE corner of layer 3 at a rate of 620 tons/hour that represents the NE-SW regional fluid flow pattern. Discharges from the model include sinks in layer 1 that represent shallow fluid movement and surface discharge and sinks in layer 3 that represent deep sub-surface discharge towards the Michatoya River. About 75% of the cool fluid

coming from the NE corner is discharged through these sinks. The remaining 25%, or 156 tons/hour, is allowed to mix with hot geothermal fluid and then discharged through the shallow sinks in layer 1

Figures 3-1-4 to 3-1-7 present the observed and calculated temperature distributions in four of the layers of the model where data was available for comparison. Notice that even temperature information of wells AMJ-1 and AMJ-2 was available, this information corresponds to a reservoir under exploitation, thus the matching was referred to the pre-exploitation temperature of the AM series and AMF series wells.

The calculated temperatures in layer 1 (Fig. 3-1-7), which correspond to an elevation of +1,050 m masl, are in fair agreement with the observed data. Better matching was obtained in the area of Calderas where more reliable data exist.

Maximum temperature at this level was calculated by the model to be about 242°C with the highest value located south of AMF-1 and AMF-2.

The calculated temperatures in layer 2 (Fig. 3-1-6), which range from 60°C to 260°C, are in good agreement with the contours of the measured temperature. Note that the temperature data available for the production area in this layer as well as subsequent layers are limited to data from the four AMF.

Fig. 3-1-5 presents the measured temperature contours and the calculated contours at +450 m masl (layer 3). Again, there are only four temperature data points available for matching at this level. As seen from this figure, the temperature contours calculated by the model are in good agreement with the available measured data. To achieve this temperature distribution it was necessary to introduce recharge sources and discharge sinks in this layer to model the deep regional fluid flow system, as described above.

Fig. 3-1-4 shows the estimated temperature distributions at +150 m masl (layer 4). This figure is presented here for completeness and should not be compared in detail due to the lack of data. The measured temperature contours is also mostly estimated since very little data are available at this depth. However, the two sets of contours do have the same shape and both are consistent with the conceptual model in that the geothermal the parent fluid is originated at depth from near the two volcanoes.

3.1.3 History Matching calibration

There are three groups of well test data. The first is the data collected by INDE/ West JEC during the 1994 flow tests of AMF-1 and AMF-2. The second group is the long term well test data collected by INDE/ICA/CFE on wells AMF-1, AMF-2 and AMF-3 (reinjection) during the two years of operation of the 5 MW geothermal power plant at Calderas. The third group of data corresponds to the testing of wells AMJ-1and AMJ-2 as described here in Chapter two (refer to section 2-4). The second group of data is the most adequate and reliable set to carry out the production (history) calibration because of the length and type of data series. Thus, the production calibration was carried out using this group of data. The production period of wells AMJ-1 and AMJ-2 (one week per each of the two testing periods) was too short to provide any significant base to assess reservoir properties.

For well AMF-1 Fig. 3-1-8 and Fig. 3-1-9 presents the mass /enthalpy history and the power respectively during this long term testing period. For well AMF-2 Fig. 3-1-10 and Fig. 3-1-11 presents the mass /enthalpy history and the power respectively during this long term testing period and Fig. 3-1-12 present the injection history on well AMF-3.

Since wellhead pressure trends do not provide a representative indication of the bottom hole pressure condition, especially in a two-phase reservoir enthalpy transients measured in flowing production wells is the matching parameter to further calibrate the model in the vicinity of the production wells.

1. Well Test Matching Procedure

The initial-state calibration is not that sensitive to storage terms such as porosity. To calibrate for these terms well test or production history is used. However, well production affects more a relatively small area around the well, therefore changes in porosity or permeability may not necessarily apply to the total simulation model. In matching well test or production information, it usually necessary to promote changes only to hydraulic parameters in blocks located close to the active or observation wells.

If the well test matching requires changes to the permeability distribution over a significant area of the model, it may be necessary to re-run the initial-state model to confirm that the calculated temperature and pressure distributions are still in reasonable agreement with the measured data. If the calculated distributions no longer agree with the measured data, then the modeling process should be continued until a more consistent model is obtained, fitting both the temperature and well test data.

Well AMF-1 was assigned to layer 2 (element AD 133), well AMF-2 to Layer 3n (element AC 91) and well AMF-3 to layer 2 (element AD 174). The production elements were further subdivided to provide for a more accurate estimation of the flowing enthalpy. Once the above subdivisions were made to the grid blocks, the enthalpy transients from the production wells were matched by trial-and-error, modifying the initial-state model as required.

The response of the model to the mass extraction at wells AMF-1 and AMF-2 and mass reinjection at well AMF-3 was simulated changing the values of hydraulic properties in the production zone. After numerous trials the enthalpy of both production wells was matched.

2. Results from 1998 Flow Test Data Matching

a. Well AMF-1

For well AMF-1 the flowing records started on November 20, 1998 and the last data available is dated December 6, 2000. The well discharge is very variable because of the multi-feed conditions in the wellbore. However the water to steam ratio remains almost constant meaning that there is no much variation in the enthalpy value. The total mass flow ranges from 90 to 160 tons/hour at an enthalpy of about 1300 KJ/kg (310 kcal/kg) in average (Fig. 3-1-8). From January 2000 there is a jump in the enthalpy curve, which is assumed to be due to recording problems since the values keeps constant at the same rate.

The calculated enthalpy and flow rate histories for well AMF-1 are also shown on Fig. 3-1-8 (Black line). Taking into consideration the possible recording problem, the match was done over the initial line of enthalpy values. The enthalpy match shows that the simulated enthalpy history agrees reasonably well with the measured data over the test period.

b. Well AMF-2

For well AMF-2 the flowing records started on November 20, 1998 and the last data available is dated December 6, 2000. Well AMF-2 discharged about 110 tons/hour (total flow) at an initial enthalpy of approximately 1650 KJ/kg (394 kcal/kg) to stabilize at 100 Tons/hour at an enthalpy of 1690 KJ/Kg (403 Kcal/Kg) in average (Fig. 3-1-10).

The measured enthalpy data has been well matched by the simulation model, as shown on Fig. 3-1-10. Simulated enthalpy values follow the same trend as the measured data and the difference between the enthalpies is small.

3. Present conditions of the reservoir

The results from matching the flow test data from the Amatitlán project area are considered to be reasonable. The model was able to accurately match the enthalpy values of long-term production of wells, AMF-1 and AMF-2.

Fig. 3-1-13 shows the temperature distribution of the upper layer of the reservoir. Figs. 3-1-16 and 3-1-19 present the distribution of temperature in the production layers. As depicted in these figures there are not large variations in the shape and values from those shown by the contour maps of the natural state simulation. This means that basically the reservoir is not being overexploited.

Fig. 3-1-14 shows the pressure distribution of the upper layer of the reservoir. Figs. 3-1-17 and 3-1-20 present the distribution of pressure in the production layers. These contour maps show no apparent depletion of mass, meaning that the general recharge to the system is adequate.

The temperature and pressure contours are consistent in showing a hydraulic barrier between wells AMF-2 and AMF-4. This explains the sharp difference in measured temperatures at similar elevations. The pressure contours also depicts the existence of the system's discharge towards El Cedro.

Fig. 3-1-15 shows the steam saturation distribution of the upper layer of the reservoir. Figs. 3-1-18 and 3-1-21 present the distribution of the steam saturation in the production layers. These contour maps indicate a vaporization in progress in the upper layers due to the poor vertical permeability in the area of wells AMF-1 and AMF-2. This simulated vaporization is in agreement with the chemistry and testing of well AMJ-2 that encountered a lower temperature steam feed zone.

3.1.4 Forecasting and field potential

The reservoir model, once calibrated as explained above, was subject to exploitation simulations to forecast its response. As part of the activities for the Fiscal Year 2000, the exploitation scenario was set to test the capacity of the

reservoir to sustain a power plant of standard size. A 50 MW plant, Double flash type was used for this purpose. These results can be found in the Interim Report to JICA of March 2001.

The Terms of Reference for the Fiscal Year 2001 ask for the analysis of three scenarios (refer to Fig. 3-1-22). The exploitation of the reservoir is done in all cases from the inside of the Calderas depression. In the following chapter two alternative P/P locations are discussed. One inside the Calderas depression and the second is a site close to INDE's warehouse at El Cedro. The scenarios are:

1. Production of only 20MW
2. Production of 40 MW in two steps. 20 initial MW and after 3 years the second step of 20 MW.
3. Production of 40 MW with two units of 20 MW.

The total existing power potential in wells AMF-1m AMF-2, AMJ-1 and AMJ-2 is not sufficient to generate the target power output of either scenario. Additional and spare drilling is required. Targets for future drilling (production and reinjection) were selected. The position of the drilling pads and targets are presented in Fig. 3-1-23.

The forecast simulation was carry out by letting the production wells to produce at constant wellhead pressure by allowing the mass flow to vary. By using the thermodynamic characteristics of the elements where production wells were assigned, first, a "kh" value was calculated per existing production well. The procedure is a trial and error procedure and was repeated until measured mass flow (steam and water) could be reproduced for the several wellhead pressures the well testing was done. The calculations were done using a wellbore simulator.

These "kh" values were later used to estimate, at the end of each time step, the mass production of simulated wells using thermodynamic properties of production elements delivered by the reservoir simulator. The make up (MKU) wells were assigned the "kh" value of the nearest existing production well. Therefore, the resulting data set was the steam and water produce by wells during the exploitation time. Power output at wellhead was calculated for condensing - single flash technology and the variation of the power per well and consolidated of all wells was tabulated. When the targeted power output was not reached because of well production decline, a new production element (production well) was activated.

The total simulation time was 25 years. The consolidated produced mass flow and enthalpy permitted the calculation of he amount of separated water to be reinjected. The total separated water was divided by the number of active reinjection wells in order to calculate the reinjection mass per reinjection well. To check for the need of additional reinjection wells, the water level at each reinjection well was estimated. When the water level raised up the wellhead of close to it, a new reinjection element (reinjection well) was activated.

3.1.5 Results of forecasting

Because the conditions at which the reservoir has to respond will differ for the three scenarios, three independent runs were carried out, following the results are described

1. **Scenario 1: 20 MW**

   Fig. 3-1-24 shows the estimated power output for the existing wells and one additional production well. Fig. 3-1-25 shows the estimated power output for each of the wells contributing to the power out put.

   The reservoir is able to sustain the 20 MW power plant without much difficulty with the planned number of production and reinjection, however it is recommended to drill one production and one reinjection spare wells as indicated in Fig. 3-1-22 for scenario-1.

2. **Scenario 2: 20 MW + 20MW**

   Fig. 3-1-26 shows the estimated power output for the existing wells and one additional production well. Fig. 3-1-27 and Fig. 3-1-28 shows the estimated power output for each of the wells contributing to the power out put.

   The reservoir is able to sustain the 20 MW initial and 20 MW additional power plants without much difficulty with the planned number of production and reinjection, however it is recommended to drill one production and one reinjection spare wells as indicated in Fig. 3-1-22 for scenario-2.

3. **Scenario 3: 40 MW**

   Fig. 3-1-29 shows the estimated power output for the existing wells and one additional production well. Fig. 3-1-30 and Fig. 3-1-31 shows the estimated power output for each of the wells contributing to the power out put.

   The reservoir is able to sustain the two 20 MW power plants without much difficulty with the planned number of production and reinjection, however it is recommended to drill one production and one reinjection spare wells as indicated in Fig. 3-1-22 for scenario-3.

Fig. 3.1.1 Reservoir Simulation Methodology(貯留層シミュレーション手法)

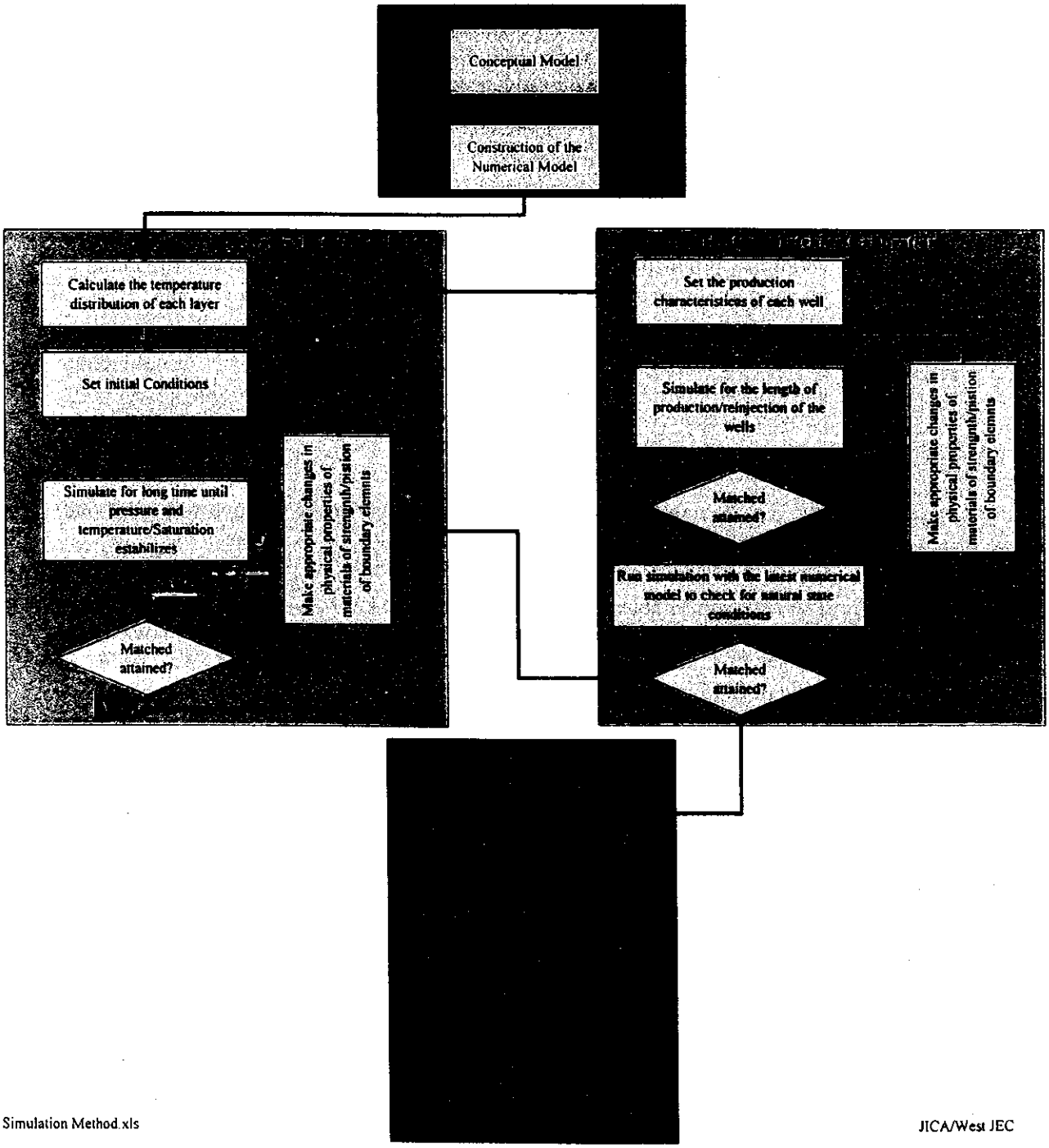

Simulation Method.xls

JICA/West JEC

Fig. 3.1.1 Reservoir Simulation Methodology (貯留層シミュレーション手法)

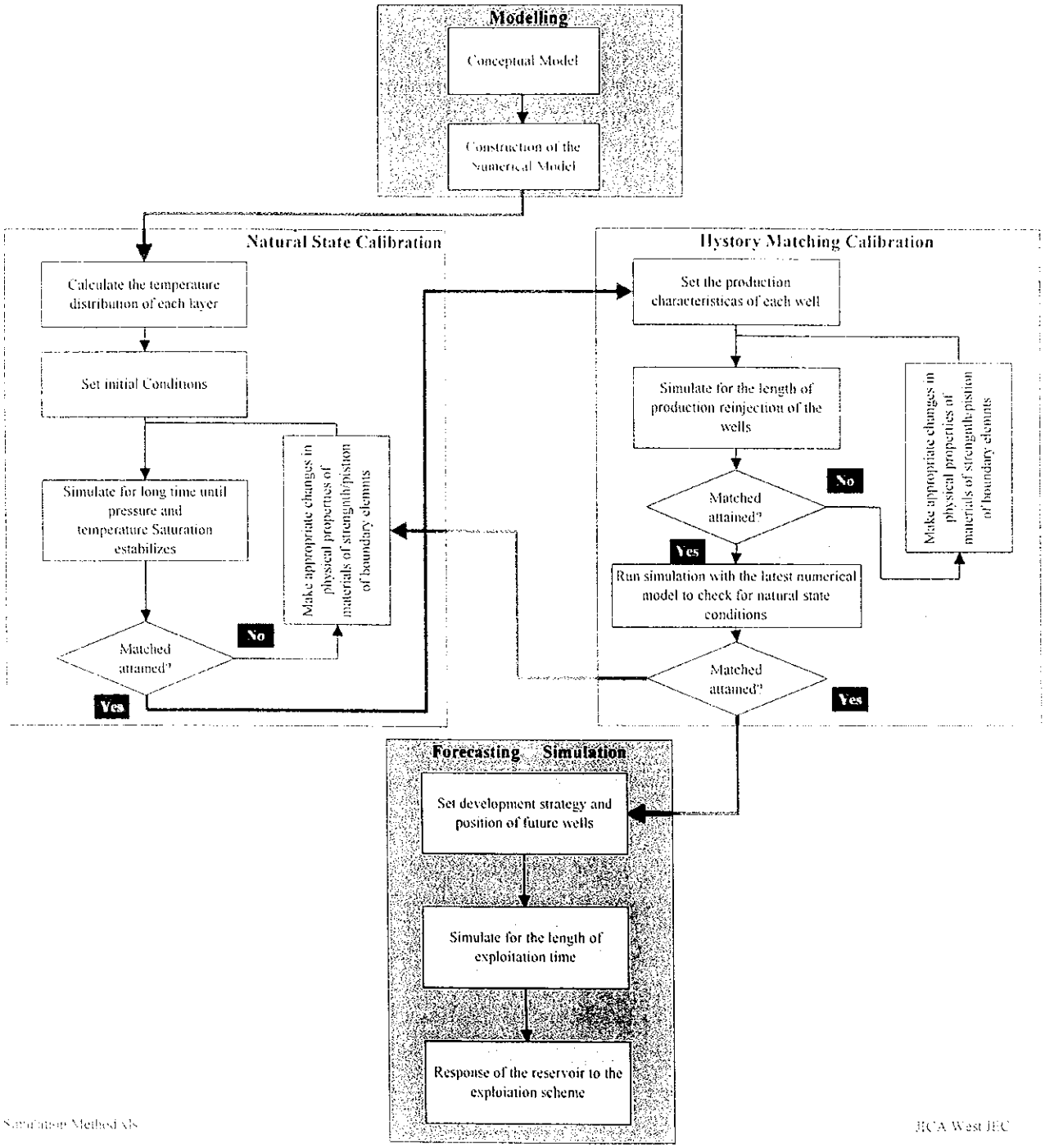

Saturation Method AS

JICA West JEC

Amatitlan Geothermal Field Reservoir Simulation

Fig. 3-1-2 **Control volume and grid used to represent the Amatitlan reservoir**
アマティトラン地熱貯留層数値モデルのブロック分割

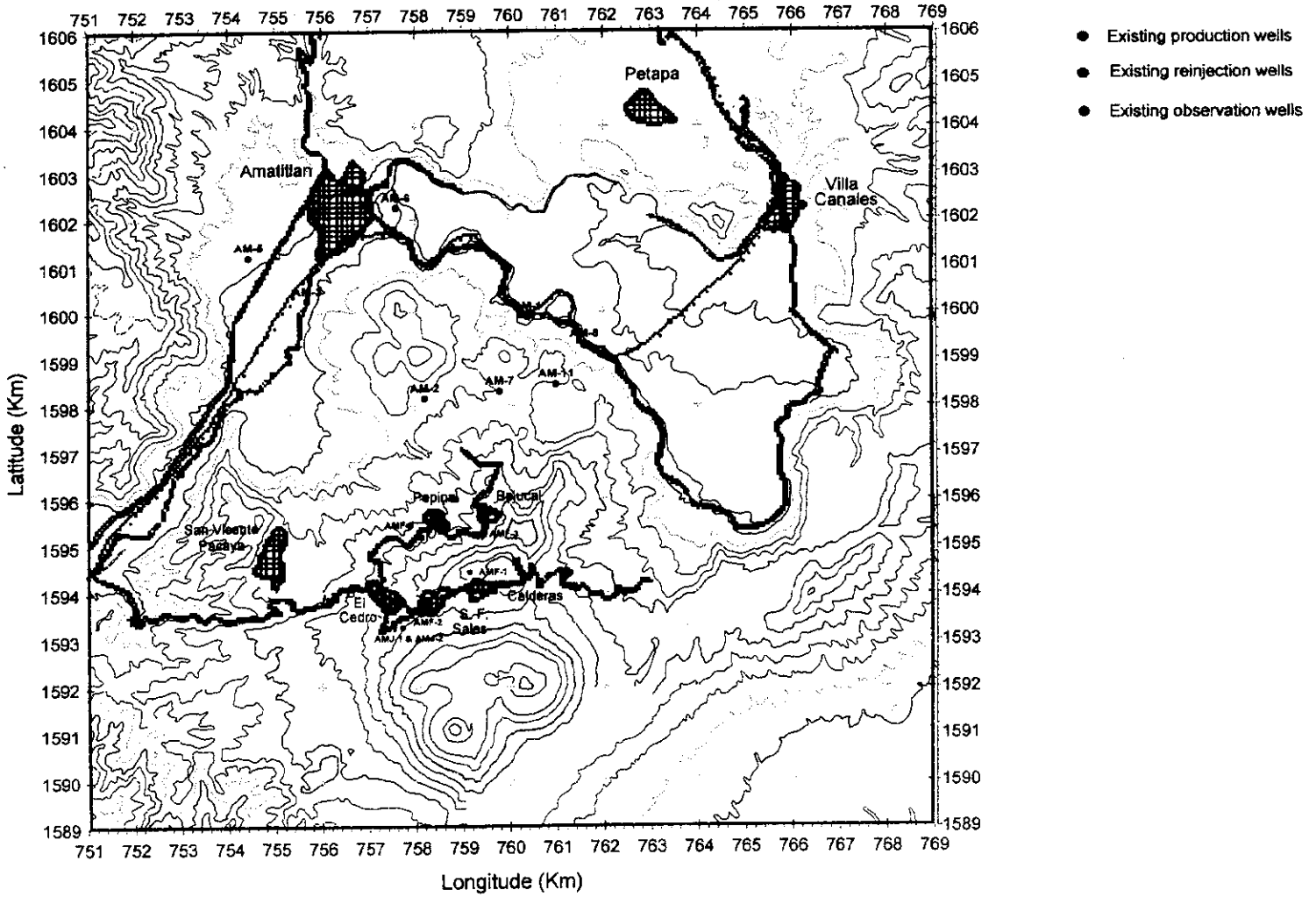

ei-2t.surf

INDE/West Jec

Amatitlan Geothermal Field Reservoir Simulation

Fig. 3-1-2 Control volume and grid used to represent the Amatitlan reservoir
アマティトラン地熱貯留層数値モデルのブロック分割